

**NASA CONTRACTOR  
REPORT**

**NASA CR-748**



**NASA CR-74**

0099830



TECH LIBRARY KAFB, NM

LOAN COPY: RETURN TO  
CIVIL ENGINEERING  
KRECHERD AFB, TEXAS

**WAKES, THEIR STRUCTURE  
AND INFLUENCE UPON  
AERODYNAMIC DECELERATORS**

*by Igor M. Jaremenko*

*Prepared by*

**GOODYEAR AEROSPACE CORPORATION**

**Akron, Ohio**

*for Langley Research Center*

**NATIONAL AERONAUTICS AND SPACE ADMINISTRATION • WASHINGTON, D. C. • APRIL 1967**



0099830

NASA CR-748

WAKES, THEIR STRUCTURE AND INFLUENCE UPON  
AERODYNAMIC DECELERATORS

By Igor M. Jaremenko

Distribution of this report is provided in the interest of  
information exchange. Responsibility for the contents  
resides in the author or organization that prepared it.

Prepared under Contract No. NASw-1288 by  
GOODYEAR AEROSPACE CORPORATION  
Akron, Ohio

for Langley Research Center

NATIONAL AERONAUTICS AND SPACE ADMINISTRATION

---

For sale by the Clearinghouse for Federal Scientific and Technical Information  
Springfield, Virginia 22151 - CFSTI price \$3.00



### ACKNOWLEDGMENTS

The author is indebted to F. A. Pake, Manager, Flight Dynamics, and F. R. Nebiker, Manager, Recovery Systems, of Goodyear Aerospace Corporation for their useful comments and help in putting the manuscript in its final form.



## ABSTRACT

The macro- and microstructure of the wake flow is presented covering the present state of the art of wake research. The decelerator-in-the-wake phenomenon is explained, and attempts to predict the influences of a wake on decelerator performance and design are described. It is shown that since no rigorous analytical treatment is available for this flow regime, the solutions are either approximate or similar. A summary of the experimental data concerning the influence of wakes upon aerodynamic decelerators and the drag efficiency and stability of a particular decelerator behind a particular payload are given.



## TABLE OF CONTENTS

		<u>Page</u>
	LIST OF ILLUSTRATIONS . . . . .	ix
<u>Section</u>	<u>Title</u>	
I	INTRODUCTION . . . . .	1
II	WAKE STRUCTURE . . . . .	3
	1. Flow Classification . . . . .	3
	2. Flow Near Body . . . . .	4
	3. Conditions at the Neck . . . . .	11
III	WAKE FLOW . . . . .	13
	1. Near Wake . . . . .	13
	2. Laminar Wake . . . . .	15
	3. Wake Transition . . . . .	17
	4. Turbulent Wake . . . . .	25
	5. Wake Growth . . . . .	30
IV	PREDICTION OF THE WAKE QUALITIES . . . . .	37
	1. General . . . . .	37
	2. Theoretical Attempts . . . . .	37
	3. Experimental Attempts . . . . .	40
V	DECELERATOR IN THE WAKE . . . . .	47
VI	CONCLUSIONS AND RECOMMENDATIONS FOR FUTURE WORK . . . . .	55
	LIST OF SYMBOLS . . . . .	57
	LIST OF REFERENCES . . . . .	61





## LIST OF ILLUSTRATIONS

<u>Figure</u>	<u>Title</u>	<u>Page</u>
1	Flow Field Nomenclature at High Speeds . . . . .	5
2	Base Flow Model . . . . .	6
3	Isoaxiometric Pitot-Pressure Traces . . . . .	18
4	Velocity Defect along Wake Centerline . . . . .	19
5	Comparison of Theory and Experiment - Simplified Laminar Theory: $x/d = 9.00$ . . . . .	20
6	Variation of Transition Distance with Reynolds Number in Wakes . . . . .	22
7	Effect of Flight Mach Number on Transition Reynolds Number for Spheres, Hemispheres, and Blunt Cones	23
8	Effect of Flight Mach Number on Transition behind Slender Bodies . . . . .	24
9	Predicted Transition Distances for Hypersonic, Axisymmetric Re-entry Bodies . . . . .	26
10	Theoretical Turbulent Wake Growth . . . . .	28
11	Velocity Defect in Wake . . . . .	33
12	Trail Width versus Trail Length for Various Bodies ( $V \approx 7000$ FPS) . . . . .	35
13	Local Flow Conditions in a Wake of a Missile in the Presence of the Ballute Decelerator . . . . .	49
14	Variation of Ballute Drag Coefficient with Payload- Ballute Separation Distance. . . . .	50
15	Effect of Air Bleed on Parachute, Model 20 behind Forebody Type II . . . . .	52

<u>Figure</u>	<u>Title</u>	<u>Page</u>
16	Drag versus $x/d$ , Hyperflo Model 1 behind Type I and II Forebodies . . . . .	54
17	Drag versus Mach Number, Hyperflo Model 2 behind Forebody Type I . . . . .	54

## SECTION I - INTRODUCTION

The wake is a flow regime that is complicated by the nature of its formation and the processes that are triggered in it after formation. Since physical aspects of the flow behind bodies have no rigorous analytical treatment, the solutions are either approximate or similar.

The decelerator, being placed in this flow regime, becomes subject to this environment, and at the same time its physical presence influences this flow field. The decelerators defined for this study are deployable aerodynamic-drag producing devices located mostly behind the bodies being decelerated and/or stabilized. It is obvious that the qualitative and quantitative properties of this regime will completely define the design and performance of a decelerator if it is completely immersed in the flow downstream of a payload. For the case of a partial immersion, the determination of boundary conditions will be important.

This report presents the state of the art of wake investigation, the decelerator-in-the-wake phenomena, and attempts to predict the influences of a wake on decelerator performance and design.



## SECTION II - WAKE STRUCTURE

### 1. FLOW CLASSIFICATION

In a very general sense, the wake is defined as the region of the flow downstream of the aft end of a body. This flow region is subject to a classification established in the fluid mechanics. Hence, the following flow definitions are applied:

1. The flow regime is usually defined in two dimensions, although the three-dimensional representation is desirable especially if a body is axi- or asymmetrical or changes the attitude.
2. It is time independent (steady state), which is a simplifying approximation; the unsteady definition, i.e., the time dependent being more appropriate.
3. The flow in the outer wake is ideal, i.e., nonviscous, incompressible, or compressible. Since it is inviscid, the vortexes are not generated and hence it is irrotational flow. The flow in the inner wake has real fluid properties (of concern here are density, viscosity, and compressibility) - thus, the possibility of vortex formation and of flow being rotational.
4. The nature of velocity distribution profiles in the region is either laminar, turbulent, or a combination of the two when the flow is transitional.

The flow region in the axial direction, downstream of the payload, is usually divided into the following subregions:

1. Base flow
2. Near wake
3. Far wake

In the radial direction the division is:

1. Outer wake
2. Inner wake

The complete flow field nomenclature is outlined in Figure 1. It is important to note that all wake studies are made for the axisymmetric type of the flow. The asymmetric flows, observed to behave in nonsimilar ways, are significant for decelerators deployed behind the payloads that are not symmetrical about the three axes.

## 2. FLOW NEAR BODY

The subregion of the flow nearest the base of a body is not classified as a wake; however, its formation and qualities have very significant impact upon the wake proper. The evaluation of the aerodynamic properties of the body (boundary layer and base region) is very important, since this predetermines the wake formation.

The starting point for this subregion is the base of the body where the boundary layer separates into the downstream direction. It extends to the neck of the wake and is defined as the base flow subregion.

Complexity of the flow processes has limited the attempted analysis mostly to the laminar cases (Chapman;<sup>1, a</sup> Baum, King, Denison;<sup>2</sup> Denison, Baum;<sup>3</sup> and Kennedy<sup>4</sup>) up until now. Based upon these sources, the base flow model is shown in Figure 2. According to the model, the flow outside the base (inviscid, high velocity, irrotational) is separated from the inner base flow (viscous, low velocity, rotational) by the shear layer, the structure of

---

<sup>a</sup>Superior numbers in the text refer to items in the List of References.

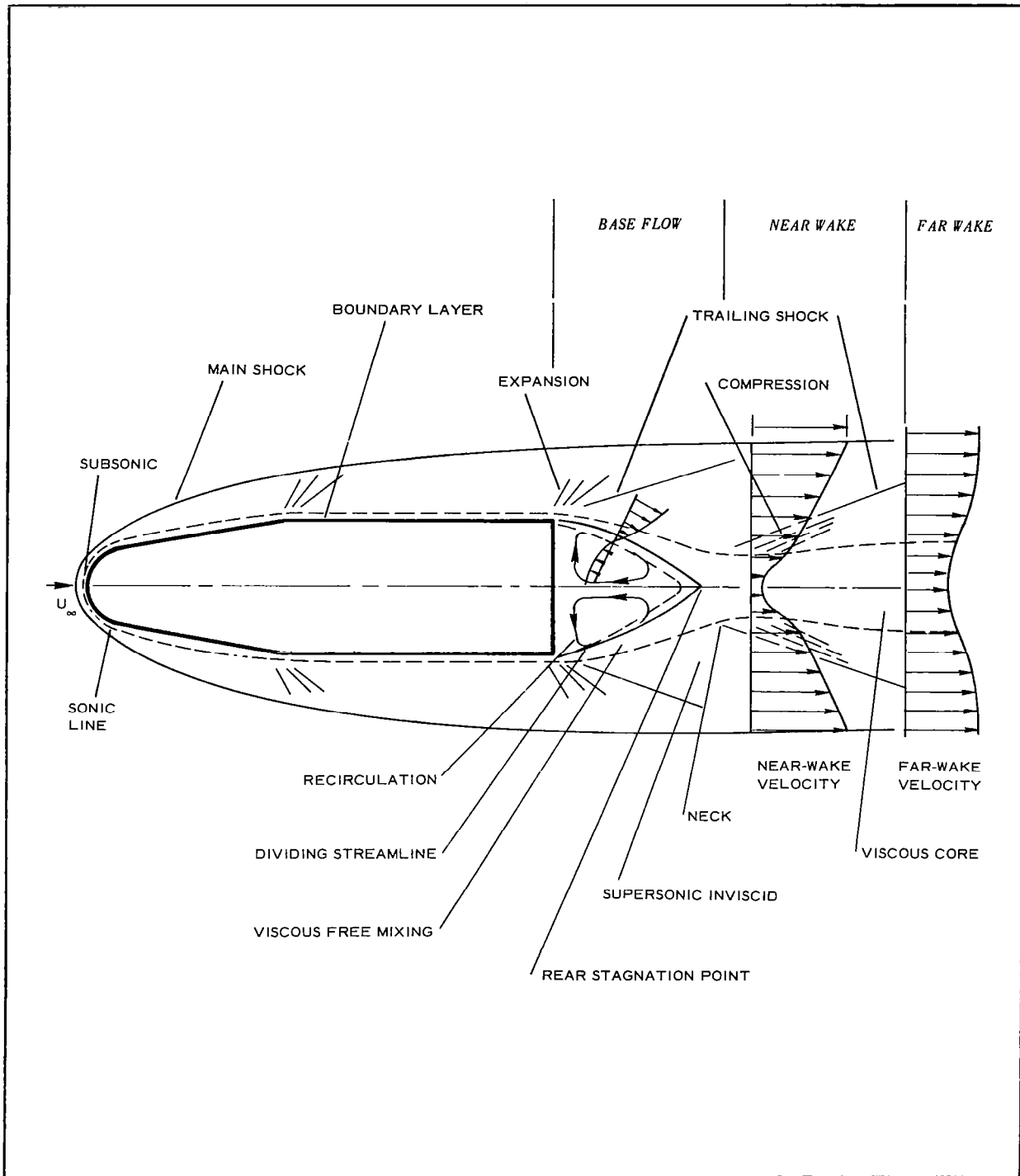


Figure 1 - Flow Field Nomenclature at High Speeds



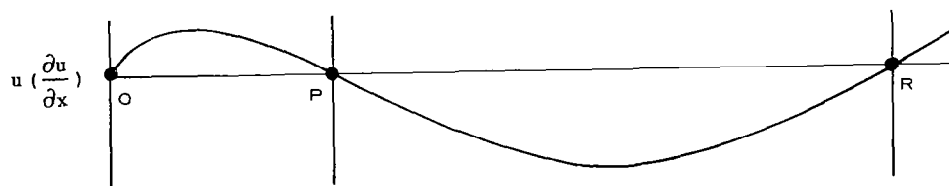
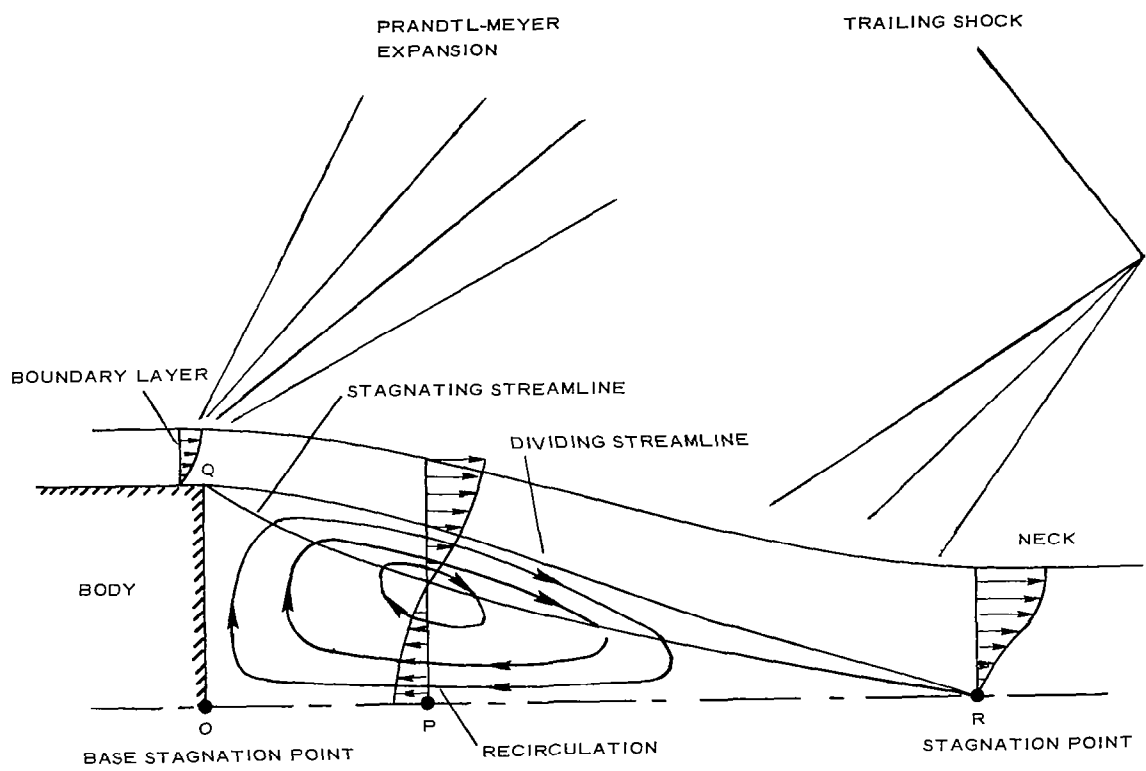


Figure 2 - Base Flow Model

which depends upon the body boundary layer. A streamline, originating at the separation point, divides (see streamline QR in Figure 2) the inner flow from the flow formed upstream. Its shape depends on the interaction with inner flow and it terminates at the rear stagnation point R under the condition of balance of shear and pressure forces. A stagnating streamline is defined as one separating the flow continuing to move downstream from that recirculating (reverse flow). Point O is a base stagnation point, hence along the OR there is a point P where shear-pressure balance occurs again, i.e.,  $\partial u / \partial x = 0$ . The product of  $u \partial u / \partial x$  in the recirculation region is plotted below the flow model. The pressure forces start to show up in the vicinity of P, are predominant in PR, and finally stagnate at R. The viscous forces predominate in OP and again downstream of R, since flow is nearly parallel to the axis and strong pressure gradients are absent. Generally, the flow in this region is governed by the equations of continuity, momentum, and energy. The solutions are simplified by the assumptions placed on the boundary conditions so that the particular solutions can be obtained mostly in two dimensions. The mathematical tools of integral and finite difference methods along with transformation techniques are employed. Chapman<sup>1</sup> carried out the solution with zero initial boundary-layer thickness. The solution applies strictly to the part where recirculating mass is entrained by the shear stresses. The method for predicting base pressure appears to give reasonable results within its applicability.

The solution of the base flow subregion is associated with behavior of the free shear layer. In Reference 3, Blasius velocity profile was converted to a Chapman distribution within a range of parameter  $S^*$ , which depends on body shape and Mach number, and is independent of Reynolds number. This in turn indicates that near the wake neck, the base pressure, wake angle, and velocity on the dividing streamline are independent of Reynolds number, but the free shear layer thickness may exhibit Reynolds number independence in laminar base flow. Further investigation (Baum, King,

Denison<sup>2</sup>) indicates that the structure of laminar base flow depends on the shape of initial separated shear layer. Kubota and Dewey<sup>5</sup> attempting the development of a constant-pressure, laminar, free-mixing layer with a finite initial thickness, arrived at the following conclusions:

1. Turning angle at the wake neck is determined by the pressure difference between the static pressure downstream of the neck and static pressure along the outer edge of the shear layer, which is the pressure rise required to stagnate the zero streamline by an isentropic compression.
2. Shear layer velocity and mass-flow profiles are subject to similar flow relationships in boundary layers. Velocity profile in the physical plane (as opposed to the hodograph plane) becomes more linear as the Mach number along the outer edge increases.
3. The total thickness of the layer increases as the Mach number at the edge increases and it penetrates more below the zero streamline.

The treatment of the two-dimensional supersonic turbulent flow in the base region (Roberts) is based upon the flow model, which splits the flow into a number of parts analyzed separately. They include the effect of corner expansion, velocity distribution in shear layer, rate of spread of shear layer, and finally, integration of parts to show how the shear layer compresses and forms a new boundary layer for a case of rear-facing step.

The mixing theory of Crocco and Lees<sup>6</sup> attempted, with some success, to explain some important aspects of the separated and reattached flows. Briefly reviewed, these aspects are as follows:

1. In a basic differential equation, there is a "critical

point" or a singularity, which in a throat-like manner, determines the base pressure.

2. The mixing rate of a turbulent flow is 5 to 10 times greater than a laminar one, hence the difference in interactions.
3. The ability of flows to support large pressure increases at high velocities, roughly proportional to the square root of mixing rate and quantity  $(M^2 - 1)^{1/4}$ , where M is the average Mach number. This indicates for example, lesser base pressure ratios as Mach number increases. Also, the pressure gradient in separating flow (base) is maximum at separation, decreasing steeply downstream. In reattachment flow (wake neck) the pressure gradient is small upstream of "reattachment" and attains the maximum at this "point."
4. The flow downstream of a blunt trailing edge of a supersonic two-dimensional body (airfoil) can attain four different regimes:
  - a. When Reynolds number is low, then not only the boundary layer but the major part of the wake neck region is laminar and the laminar mixing rate is decreasing while base pressure ratio ( $P_b/P$ ) is increasing slowly with the Reynolds number based on length.
  - b. The upstream motion of transition in the wake initiated when base pressure attains local maximum, and with Reynolds number increased it drops sharply because of a gain in mixing rate. The important phenomenon is the existence of a range of Reynolds numbers at which, although the transition is close to the base, the boundary layer on the body stays laminar. The necessary condition, however, is that the ratio of length to aft-end thickness be low (short, blunt bodies)

or the boundary layer transition Reynolds number be high and the reversibility of above is excluded. Under the conditions listed, the base pressure ratio is decreasing with decreasing boundary layer thickness while  $Re_c$  is increasing.

- c. Further motion of the transition upstream, i. e., into the boundary layer along the two-dimensional body, causes a base pressure rise due to increase in boundary layer thickness, which eventually is balanced by the decrease of local boundary layer thickness due to an increase in Reynolds number. Hence base pressure upon reaching a peak decreases with increasing Reynolds number.
- d. At high Reynolds numbers, when transition is far downstream from the base, the base pressure decreases slowly due to lower turbulent boundary layer thickness as the Reynolds number increases.

The theory of Crocco-Lees did not provide quantitative agreement with experimental results in the flow prior to separation. Later investigation (Glick)<sup>7</sup> showed that a new mixing-rate correlation function  $C(k)$  satisfies the calculations for the two-dimensional laminar supersonic flow up to separation. In addition to confirming the principle of the "dividing" streamline, it proposes the physical model according to which the transport of the viscous momentum is dominating in the domain bounded between the separation and initiation of reattachment. The process of reattachment, however, has an inviscid nature. The pressure rise during the reattachment is isentropic, which leads to inviscid recompression with no significance of the mass entrainment shown. The problem of obtaining the engineering solution for the conditions near a body still remains

to be semiempirical in nature (McCarthy<sup>8</sup> or Brown, Kramer, Smith<sup>9</sup>).

### 3. CONDITIONS AT THE NECK

The conditions at the neck can be specified in terms of a separation angle and a fictitious Mach number, which would occur if the separation at a given separation angle did not materialize. The shear layer is defined as a line along which the flow would move before the turn and initiation of the trailing shock. Then if the trailing shock angle is known (from pitot-pressure readings), the turning angle, angle of shear layer, angle of wake growth, pressure ratios, and distance from the base to turn can be estimated by application of the two-dimensional compressible flow methods. As a rule, the pitot and static pressures have high values while at the wake's neck, however, the Mach number is relatively constant at the edge. There is considerable difficulty in locating the exact axial station for the neck because of instrument limitations. Neither does the visual technique (schlieren) give the full quantitative picture.

Additional distortions are introduced when the decelerator with its connecting system is placed at or in the vicinity of the neck. The base flow subregion will be distorted. The decelerator placed at random in the neck region will be subjected to the unsteady oscillatory regime.

For analytical purposes the neck width and its momentum thickness are required for initial conditions. Based on skin friction and pressure rise at the neck, they are estimated to vary as the Reynolds number parameter based on diameter  $(Re_d)^{-1/2}$  (Lees and Hromas<sup>10</sup>).

Hence if skin friction coefficient varies as

$$c_f \approx \frac{1}{\sqrt{Re_{local}}}$$

and

$$\frac{1}{\sqrt{\text{Re}_{\text{local}}}} \approx \frac{1}{\sqrt{\text{Re}_d}},$$

then

$$\left(\frac{y}{d}\right)_{\text{neck}} \approx (\text{Re}_d)^{-1/2}$$

and

$$\left(\frac{\theta}{d}\right)_{\text{neck}} \approx (\text{Re}_d)^{-1/2}.$$

Experimentally the width is determined from the magnitudes of the pitot pressures. It is difficult however to pinpoint the exact axial station.

The momentum thickness, being defined as,

$$\theta = 2 \int_0^{\infty} \frac{\rho u}{\rho_e u_e} \left(1 - \frac{u}{u_e}\right) dy \quad (1)$$

can be calculated from the experimental data or from the boundary layer type equations.

### SECTION III - WAKE FLOW

#### 1. NEAR WAKE

In development of the near wake model, the two most important concepts are: (1) requirement by the conservation of mass that all fluid within the base flow (i. e., original plus that entrained by the shear layer) must be accounted for at the neck; and (2) the shear layer mixing rate determines the pressure rise required to satisfy condition (1) almost exclusively.

The model (Dewey<sup>11</sup>) for the near wake is defined along the principles of mass and momentum conservation observed on the dividing streamline. The formation of viscous mixing layer is due to the boundary layer separation in the immediate vicinity of the body's aft end by pressure and viscous forces. As it moves along, it entrains some additional mass from the inviscid flow on its outer edge and another increment from the lower edge, i. e., the base flow. The potential growth of the layer increases the Mach number and velocity along the dividing streamline ( $\psi = 0$ ) due to momentum transfer. In two-dimensional flow its path is approximated by the straight line changing to the convex in axisymmetric flow. For the case where separation point is steady, the angle between the shear layer and the axis is specified. Thus, the Mach number, velocity, and pressure on the outer edge (inviscid) are also known.

The pressure rise required to stagnate the dividing streamline is a function of the inviscid flow deflection, or

$$(P_l - P_e) \approx \theta_s$$

It is also shown by Dewey<sup>11</sup> that the ratio of the Mach number along the dividing streamline ( $M^*$ ) over the Mach number at outer edge at the neck is a function of the parameter



$$\xi(\ell) = \left(\frac{\ell}{\theta_o}\right)^2 \frac{\ell}{\text{Re}_{e,\ell}}, \quad (2)$$

where

$\ell$  = distance along shear layer, and

$\theta_o$  = initial momentum thickness.

The  $M^*$  magnitude is decreasing as  $\ell$  grows with  $\xi(\ell)$ . Then for each  $M^*$  required by mass conservation, there is equivalent  $M^*$  given by mixing, both referred to the particular value of  $\xi$ .

The other important characteristics of the shear layer are:

1. As the Reynolds number ( $\text{Re}_{e,\ell} = \rho_e u_e \ell / \mu_e$ ) is increasing, the shear layer thickness is decreasing. The same holds for the readjustment regions at separation and neck.
2. It represents a surface with essentially constant pressure.
3. Sharp corner separation results in fuller initial velocity profile and larger mixing rate than a separation from a convex surface.

Comparison of the supersonic near wake behind the two-dimensional and axisymmetric bodies indicates three features:

1. Dominant role of viscosity at the neck for wake shock admittance in axisymmetric flow but not in two-dimensional flow.
2. Constant pressure surface converging toward the wake axis is convex for axisymmetric flow but straight for two-dimensional flow.

3. Thickness of the free shear layer in axisymmetric flow is larger than that in two-dimensional flow.

The initial wake velocity profile half-thickness is approximately related to that at separation by:

$$\left(\frac{\delta_w}{d}\right)^2 \cong \left(\frac{\delta_B}{d}\right),$$

where

$\delta_w$  = initial wake thickness,

$\delta_B$  = at separation, and

$d$  = body diameter.

In conclusion, for the solution of the near-wake problem, the initial and edge conditions that are obtained in a combined analytical-empirical effort must be known.

## 2. LAMINAR WAKE

The solution of the laminar wake is based on the assumption that viscous boundary layer equations for continuity, momentum, and energy apply:

$$\frac{\partial(\rho u)}{\partial x} + \frac{\partial(\rho v)}{\partial y} = 0 \quad (3)$$

$$\rho u \frac{\partial u}{\partial x} + \rho v \frac{\partial u}{\partial y} = \rho_e u_e \frac{d u_e}{dx} + \frac{\partial}{\partial y} \left( \mu \frac{\partial u}{\partial y} \right) \quad (4)$$

$$\frac{\partial p}{\partial y} = 0 \quad (5)$$

$$\rho u \frac{\partial H}{\partial x} + \rho v \frac{\partial H}{\partial y} = \frac{\partial}{\partial y} \left( \frac{\mu}{\sigma} \frac{\partial H}{\partial y} \right) - \frac{\partial}{\partial y} \left( \frac{1-\sigma}{\sigma} \mu u \frac{\partial u}{\partial y} \right). \quad (6)$$

The two-dimensional case, where

$$H = h + \frac{1}{2} u^2 \quad (\text{total enthalpy})$$

and

$$\sigma = \frac{c_p \mu}{k} \quad (\text{Prandtl number}),$$

has the following boundary conditions:

$$u(x, \pm \infty) = u_e(x);$$

$$\frac{\partial u}{\partial y}(x, 0) = 0$$

and

$$H(x, \pm \infty) = H_e;$$

$$\frac{\partial H}{\partial y}(x, 0) = 0.$$

Pallone, Erdos, and Eckerman<sup>12</sup> obtained the following expressions for the velocity and enthalpy profiles:

$$\frac{u}{u_e} = 1 + e^{-\frac{\eta}{(1-\eta)}} \sum_{n=0}^n a_n \eta_n \quad (7)$$

and

$$\frac{H}{H_e} = 1 + e^{-\frac{\eta}{(1-\eta)}} \sum_{n=0}^{n+1} b_n \eta_n, \quad (8)$$

where the  $\eta$  is a transformed independent variable,

$$\eta = \left[ \frac{(j+1)}{\delta_t^{j+1}} \int_0^r \frac{\rho}{\rho_e} r^j dr \right] \frac{1}{(j+1)}, \quad (9)$$

and the wake thickness is

$$\delta_t = \left[ (j+1) \int_0^\delta \frac{\rho}{\rho_e} r^j dr \right] \frac{1}{(j+1)}, \quad (10)$$

where

$$j = \begin{cases} 0 & \text{two-dimensional flow} \\ 1 & \text{axisymmetric flow,} \end{cases}$$

$r$  = normal coordinate from axis  
or plane of symmetry.

Typical pitot pressure traces in laminar wake and velocity defect along the centerline are shown in Figures 3 and 4. The comparison of the simplified laminar-wake theory with experimental results for the normalized distributions of velocity, static enthalpy, and total enthalpy from McCarthy<sup>8</sup> are given in Figure 5.

### 3. WAKE TRANSITION

Transition in the wake from the laminar velocity profile to a turbulent one generally depends on a Reynolds number and Mach number, which are based on the relative velocity of the wake. Essentially, the problem is to define the stability of the flow since knowing the stability boundaries the transition point can be predicted. Thus, according to Gold<sup>13</sup> the following affect the stability of the wake.

1. The two-dimensional inviscid wake can be stable or unstable as a function of temperature. Then as the critical Mach number increases, the temperature increases and so does the possibility of subsonic disturbances. Hence, if the Mach number is below critical, stability is indicated.
2. A hot wake shows better stability than a cool one, provided the relative Mach number stays below critical.
3. The axisymmetric inviscid compressible wake stability is dependent upon the Reynolds shear stress

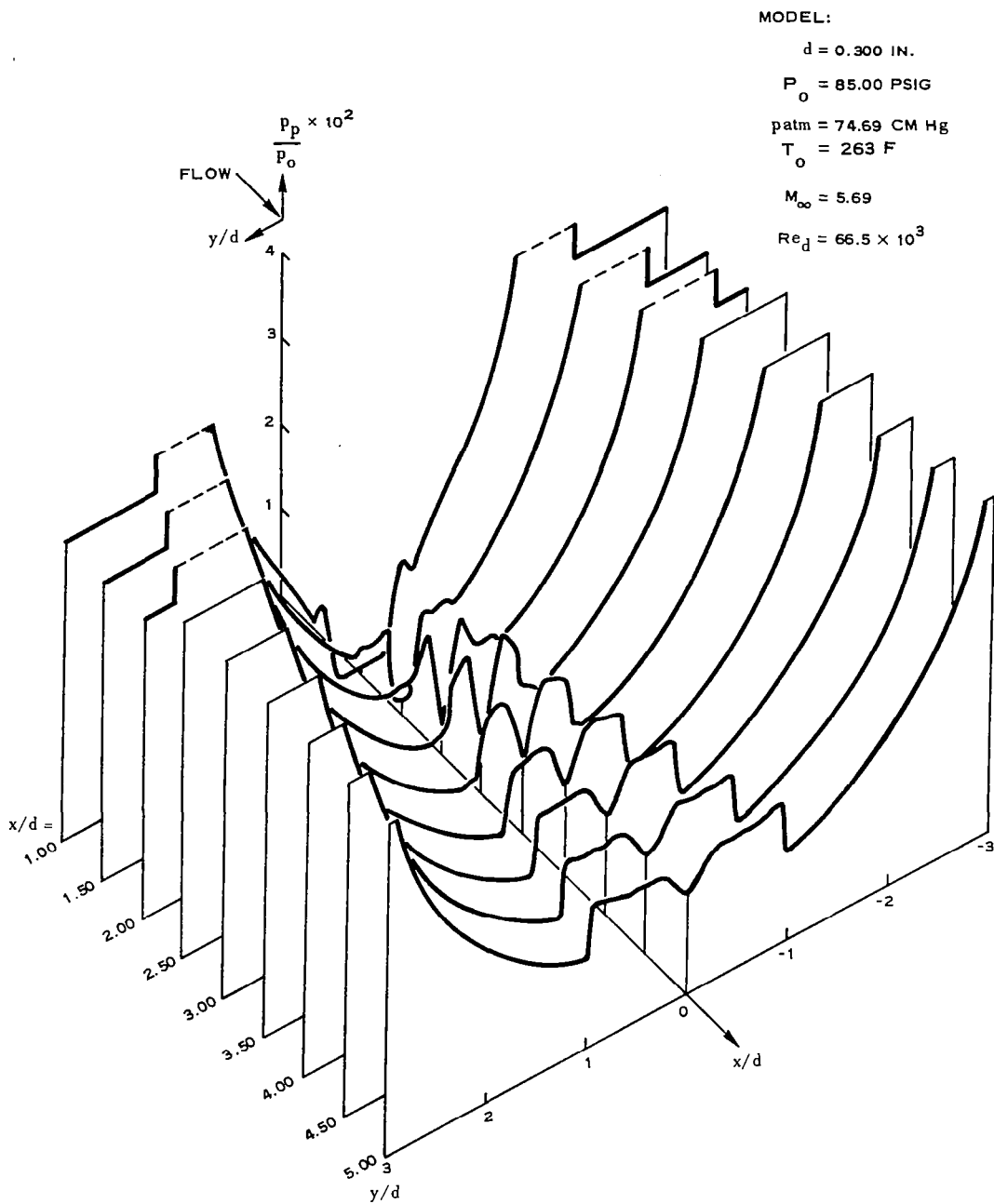


Figure 3 - Isoaxiometric Pitot-Pressure Traces<sup>8</sup>

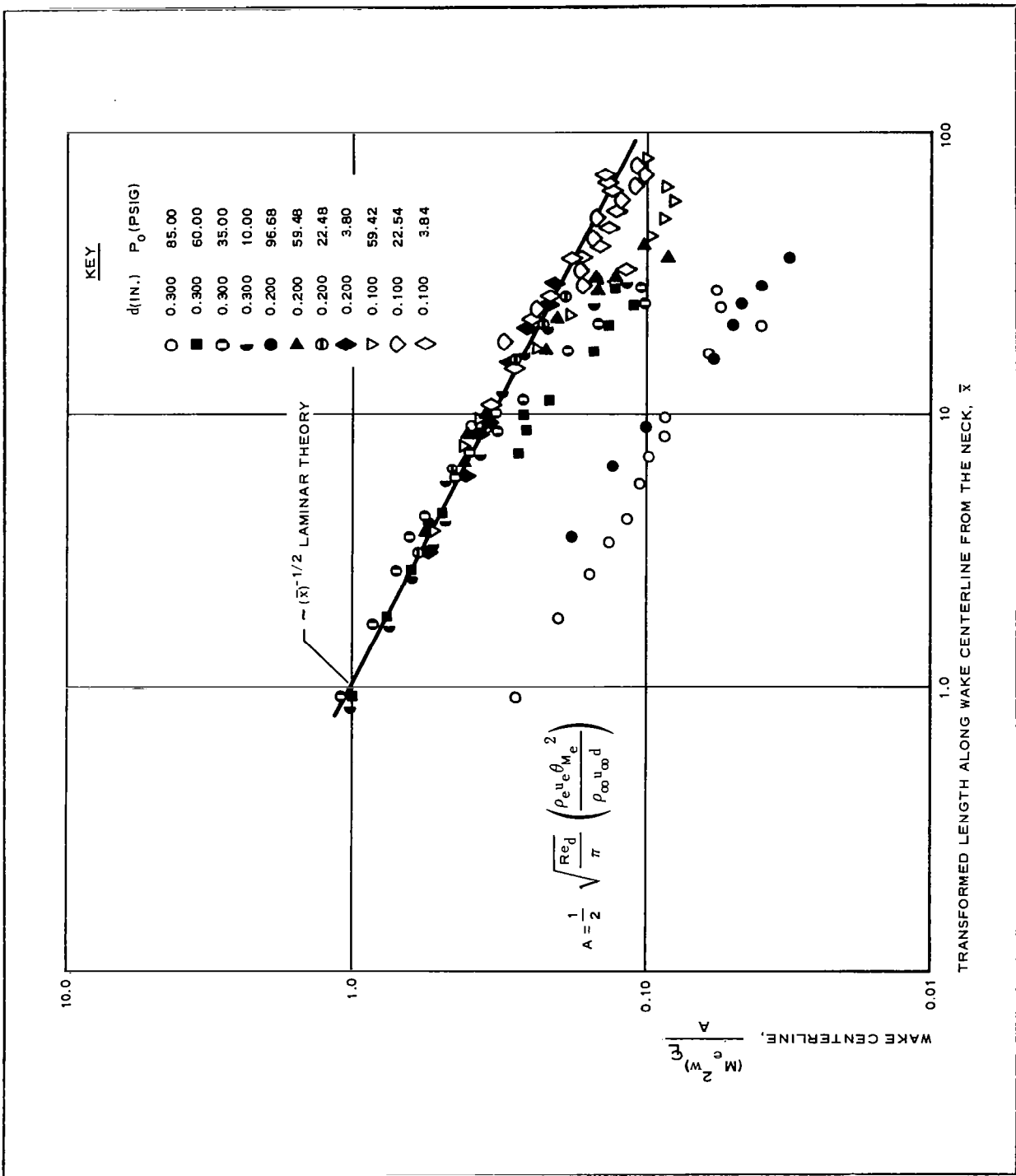
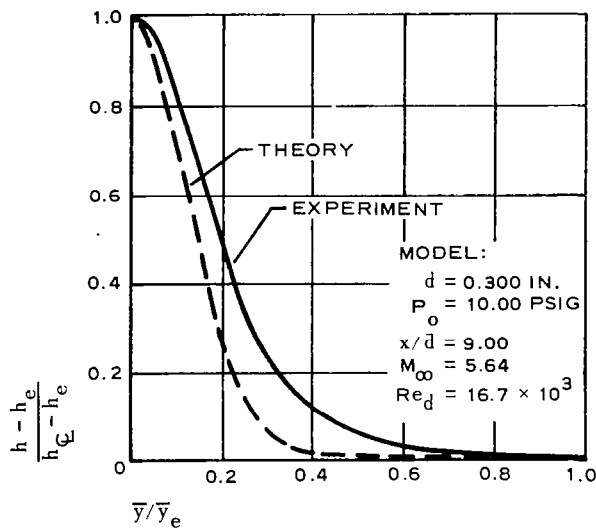
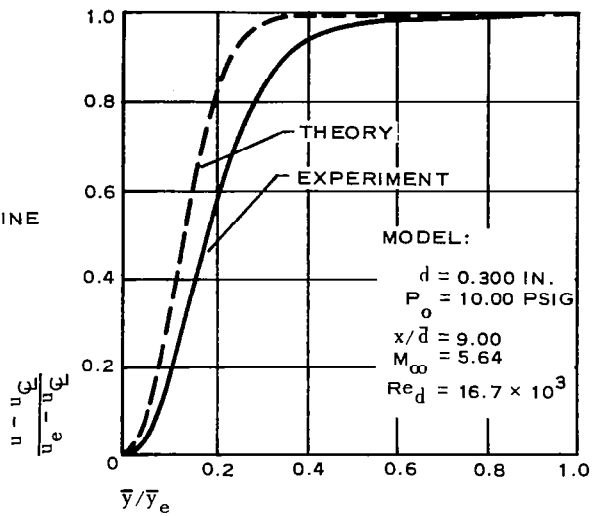


Figure 4 - Velocity Defect along Wake Centerline<sup>8</sup>

$v$  = VELOCITY PARALLEL TO WAKE CENTERLINE  
 $\bar{y}$  = LENGTH NORMAL TO WAKE CENTERLINE,  
 TRANSFORMED



$h$  = STATIC ENTHALPY  
 $H$  = TOTAL ENTHALPY  
 $( )_e$  = AT WAKE OUTER EDGE

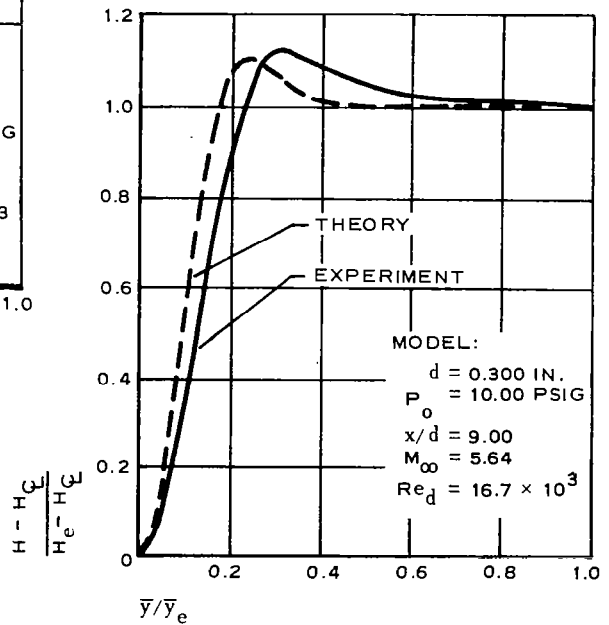


Figure 5 - Comparison of Theory and Experiment - Simplified Laminar  
 Theory:  $x/d = 9.00^8$

near the critical point, the presence of which is destabilizing. The direction of the density-vorticity gradient is also important.

4. The stability of the incompressible axisymmetric wake flow depends on the so-called wave number derived from the Batchelor and Gill analysis.

Again Van Driest and Blumer<sup>14</sup> consider the boundary layer transition on the basis of the limiting value of the ratio of local inertial stress to local viscous stress somewhere in the flow after presence of which transition takes place. The compressibility effects indicate a decrease in transition Reynolds number with increasing Mach number. If heat transfer is taken into consideration at  $M = \text{constant}$ , the transition  $Re$  will increase with decreasing wall temperature.

Thus, although several approaches have been taken, at present there is no sound theory that will explain the transition phenomena. The experimental measurements usually provide answers to a particular problem, but the attempts to correlate them to obtain parameters that could in a general way predict the phenomena are far from being satisfactory as exemplified by References 15 and 16.

In general, transition characteristics behind the blunt and slender bodies will be different. The blunt bodies have strong flow gradients due to bow shocks, which are absent for the case of slender bodies.

The lower boundary for the transition Reynolds number as estimated by Lees<sup>17</sup>

$$\left( Re_{\infty, d} \right)_{\min}^{Tr} \approx 3 \times 10^4 \text{ for slender bodies}$$

and

$$\left( Re_{\infty, d} \right)_{\min}^{Tr} \approx 5 \times 10^4 \text{ for blunt bodies .}$$



Below those values the flow is laminar. Demetriades defined the transition Reynolds number by the following expression

$$Re_{\infty, Tr} = \frac{(X_{Tr} - X_o) \rho_{\infty} u_{\infty}}{u_{\infty}}, \quad (11)$$

where

$X_{Tr}$  = transition distance,

$X_o$  = sticking distance.

The sticking distance is measured from the base and indicates the stability of the flow under certain conditions.<sup>18</sup>

Various attempts to represent the correlating parameters for slender and blunt bodies are shown in Figures 6 through 8, indicating current trends.

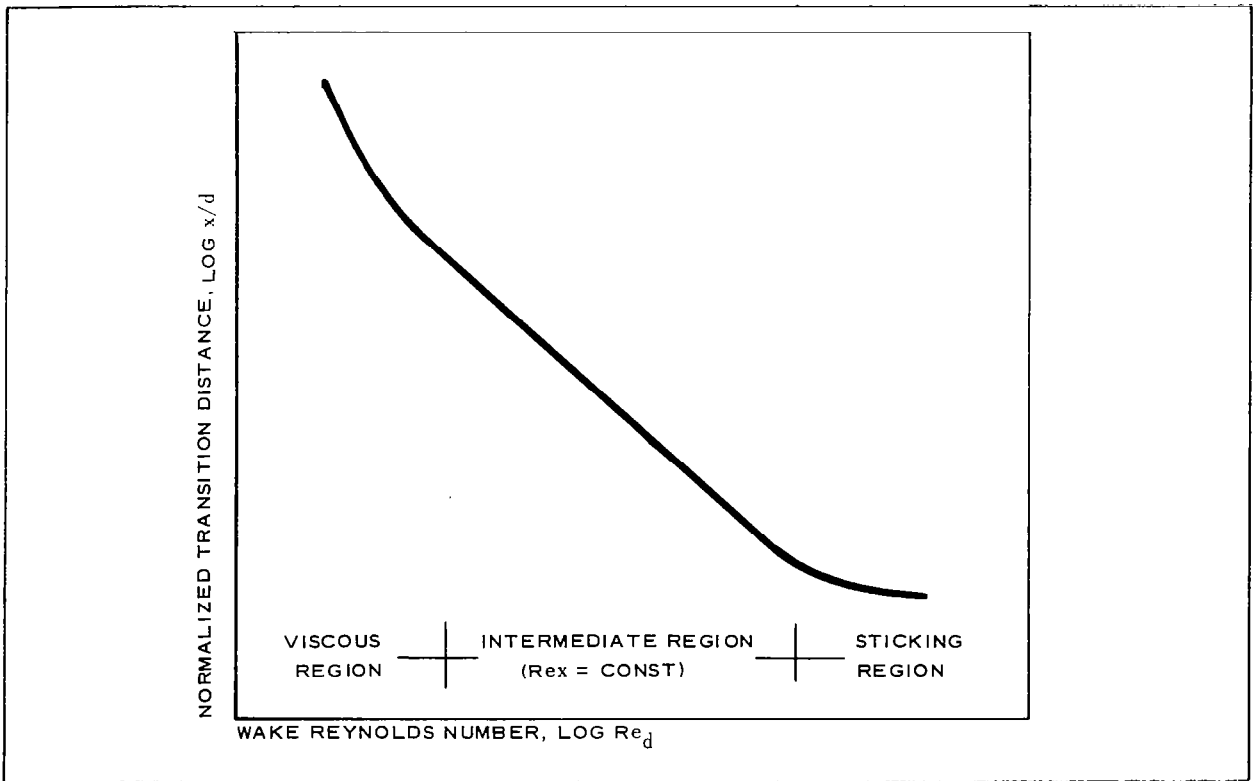


Figure 6 - Variation of Transition Distance with Reynolds Number in Wakes<sup>17</sup>

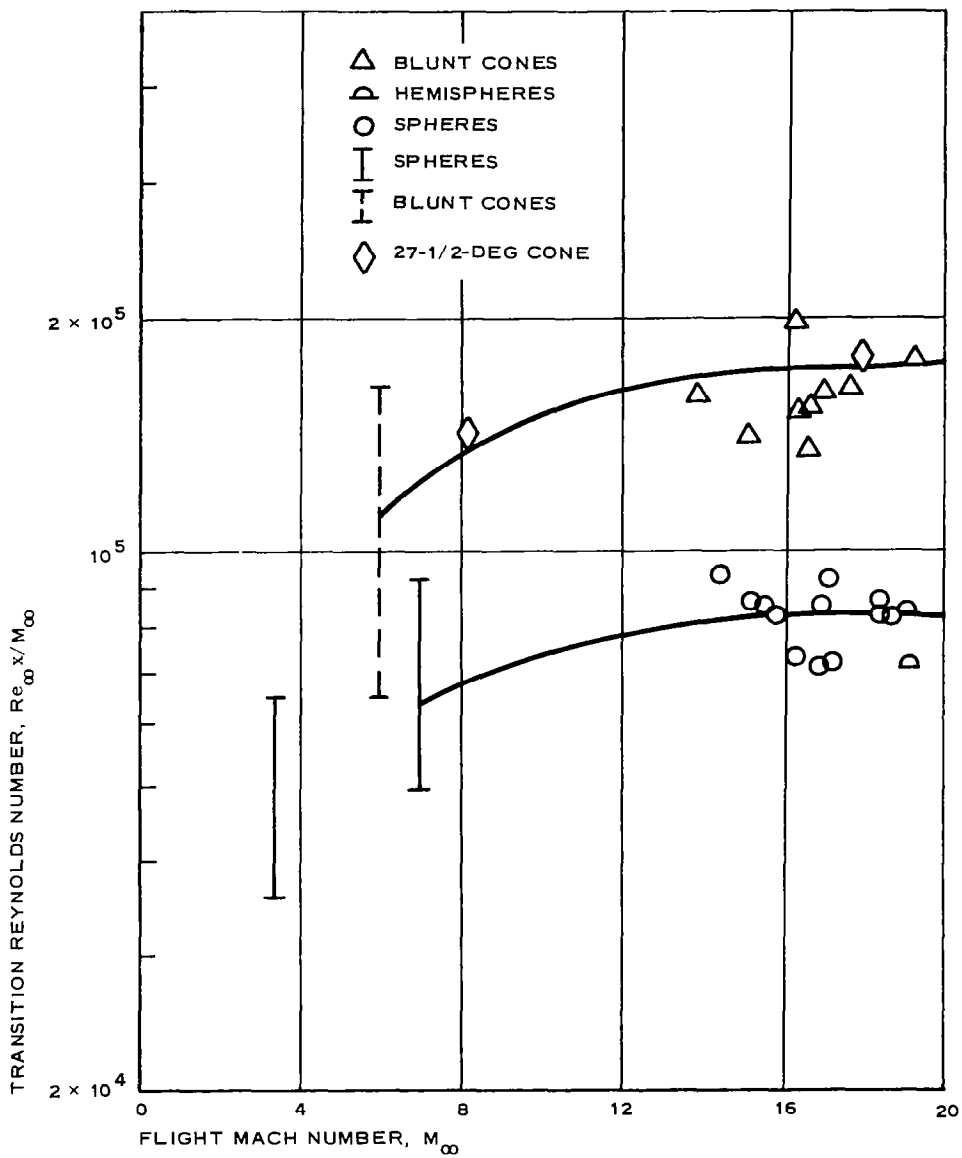


Figure 7 - Effect of Flight Mach Number on Transition Reynolds Number for Spheres, Hemispheres, and Blunt Cones<sup>17</sup>

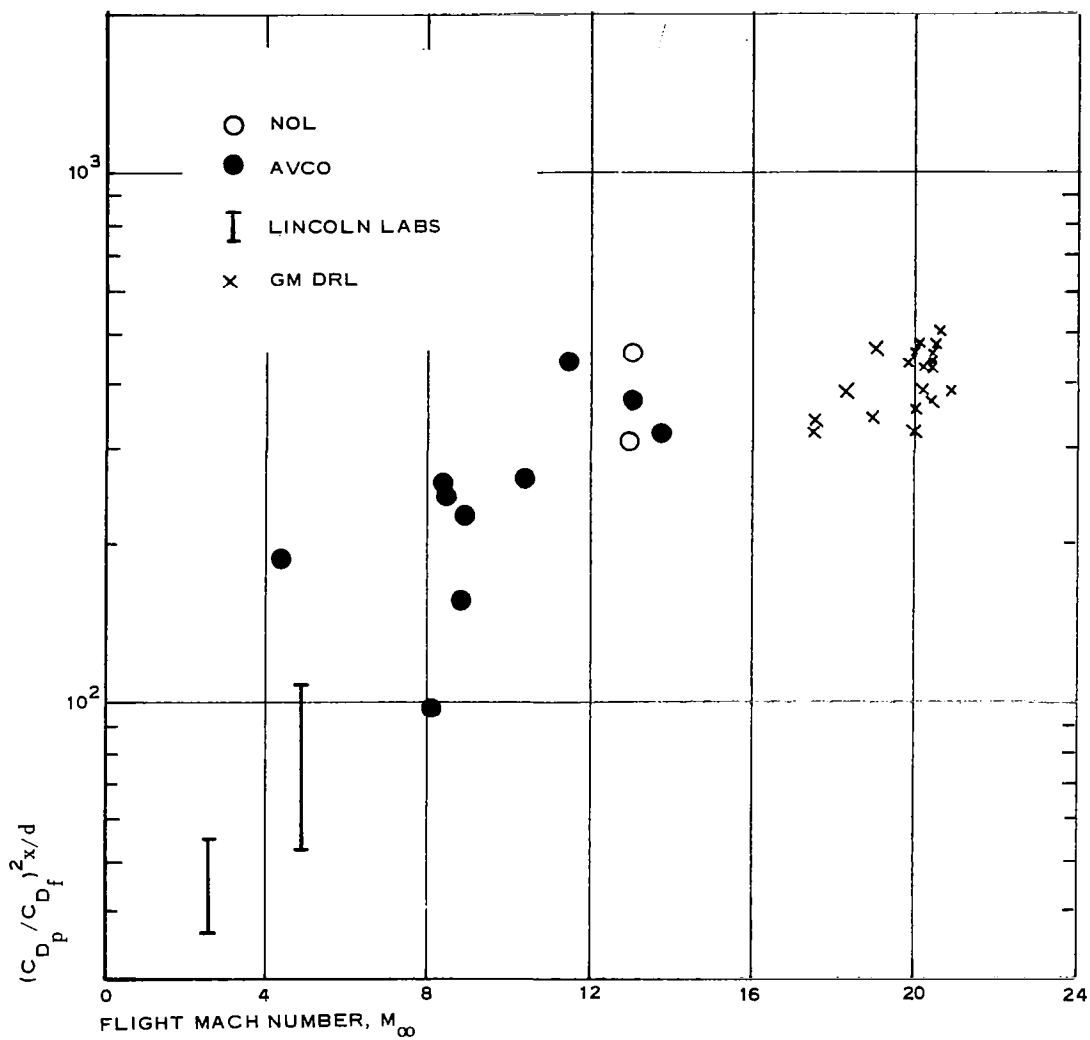


Figure 8 - Effect of Flight Mach Number on Transition behind Slender Bodies<sup>17</sup>

The transition distances behind the blunt bodies in general are independent of shape. The slender bodies show a definite shape effect. The process of transition occurs somewhat abruptly behind blunt bodies, while behind the slender bodies it extends over several diameters. In all cases (Wilson<sup>19</sup>) the independence of transition distance from body size and flight speed is indicated. The correlation breaks down at high Reynolds numbers where turbulence originates in the recompression region.

The important differences between the inviscid and viscous wake are due to the fundamental differences of the flow fields behind the blunt and slender bodies. For the slender bodies the field is boundary-layer dominated and for the blunt one it is shock-wave dominated. The transition distances for hypersonic axisymmetric bodies can be correlated by the shape parameter such as

$$S = \frac{C_{D_f}}{C_{D_p}} \sqrt{\frac{Re_{\infty, d}}{M_{\infty}}}, \quad (12)$$

where

$C_{D_f}$  = boundary layer drag coefficient based on free stream conditions and base area,

$C_{D_p}$  = pressure drag coefficient based on the same conditions.

Based on this shape parameter, the bodies are classified as blunt or slender and transition distances are shown in Figure 9.

#### 4. TURBULENT WAKE

The preservation of uniform steady laminar wake is desirable for analytical and applicational reasons, however, its stability due to geometry, flow parameters, and physicochemical reactions cannot be retained. Consequently, the turbulent state is reached at some axial station. This axial station varies from the point where the flow separates from the body

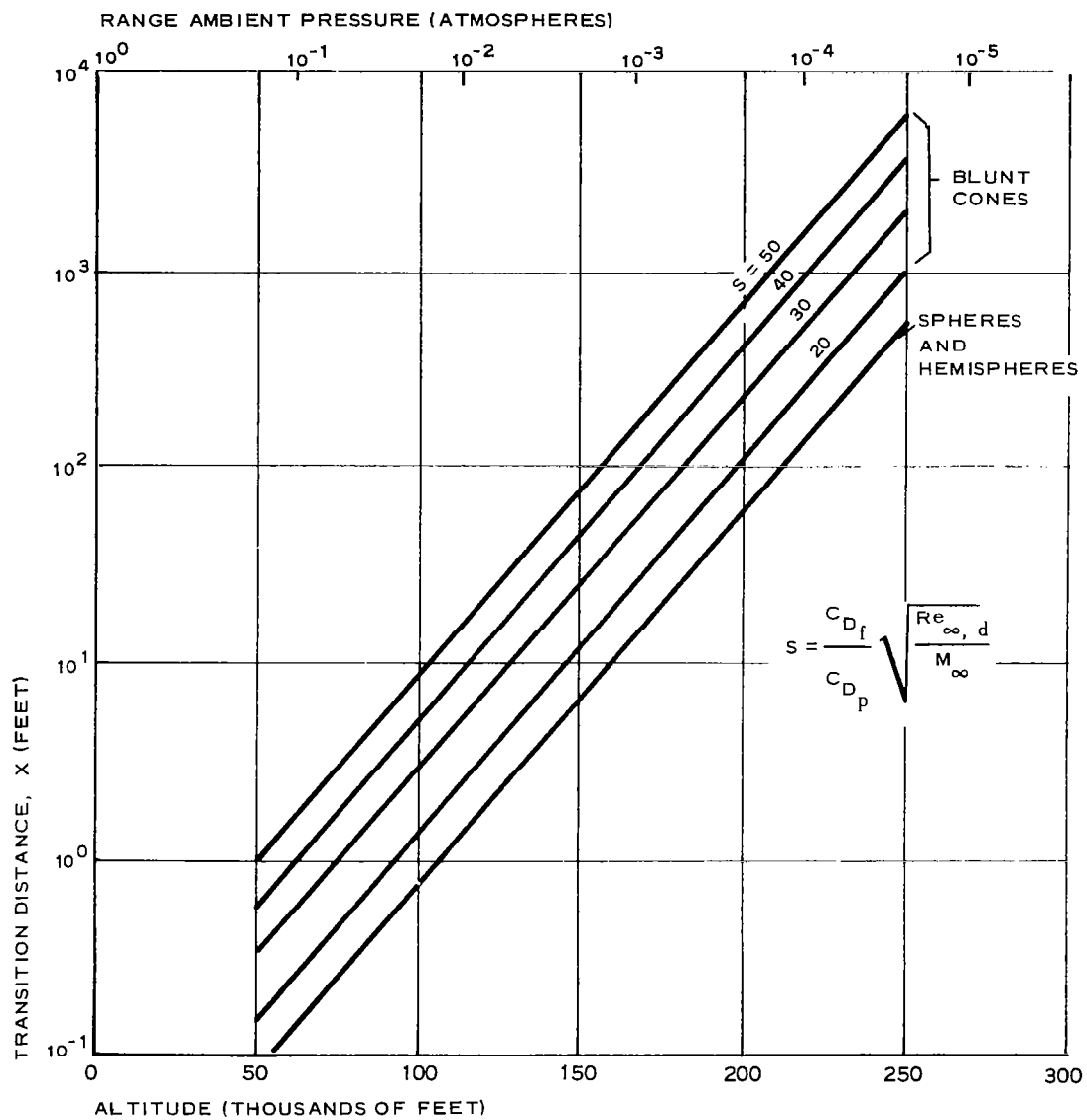


Figure 9 - Predicted Transition Distances for Hypersonic, Axisymmetric Re-entry Bodies<sup>17</sup>

(subsonic and low supersonic Mach numbers) to the position where the neck is located (high supersonic and hypersonic Mach numbers). The general physical meaning is thought to be a penetration of the inviscid flow profile by the turbulent momentum thickness of an initial width.

Theoretical attempts to describe turbulent wakes are usually extensions of the laminar results, which are coupled by the introduction of an eddy transport coefficient. This seems to predict the growth but avoids the problem of turbulent mixing, which is very important.

The condition for existence of turbulence is a sufficiently large Reynolds number and initial formation of the free shear layer as a result of the boundary layer separation. Then the wake grows, entraining the originally inviscid outer wake. The presently accepted physical model (Prou-dian, Feldman<sup>20</sup>) can be described as follows: the initial momentum of finite width, which is separated from the nonturbulent flow by a distinct front, consists of eddies of different sizes. The relatively large eddies possess the most of kinetic energy of turbulence, while the smaller ones are mostly dissipating viscous kinetic energy into heat. The contour of the core is outlined by the largest eddies, which do not contain much energy (subsonic wakes). The lifetime of an eddy decreases sharply with its size. The eddies containing energies also have short lives.

The eddies with highest velocity gradients (smallest in size) start the process of diffusion by propagating the vorticity, which is reinforced by the energy transfer from the energy carrying eddies. The process of mixing between the outer wake and the inner turbulent wake is a convection of relatively large fluid particles by the large-scale eddies introduced into the already turbulent core. The shearing of the small-scale eddies reduces the introduced inhomogeneities until the process of diffusion on a molecular scale takes over and complete dissipation is the final result.

In general, analytical treatment of the turbulent wake produced so far is for simple models, but even those are difficult to verify experimentally.

Two representative parameters, i.e., static-enthalpy and wake's width are shown in Figure 10.

The investigation of Lees and Hromas<sup>21</sup> produced some practical conclusions, which are summarized here. One assumption is that although at  $x/d$  of up to 50 the pressure has the dominant role in wake development, the enthalpy buildup and dissipation become important. The reduction of enthalpy (at  $M_\infty > 1$ ) is proportional to

$$r_n^2 \frac{\rho c_p}{k},$$

where

$$r_n = \text{nose radius.}$$

The time involved is equal to

$$t = \frac{x}{u_\infty},$$

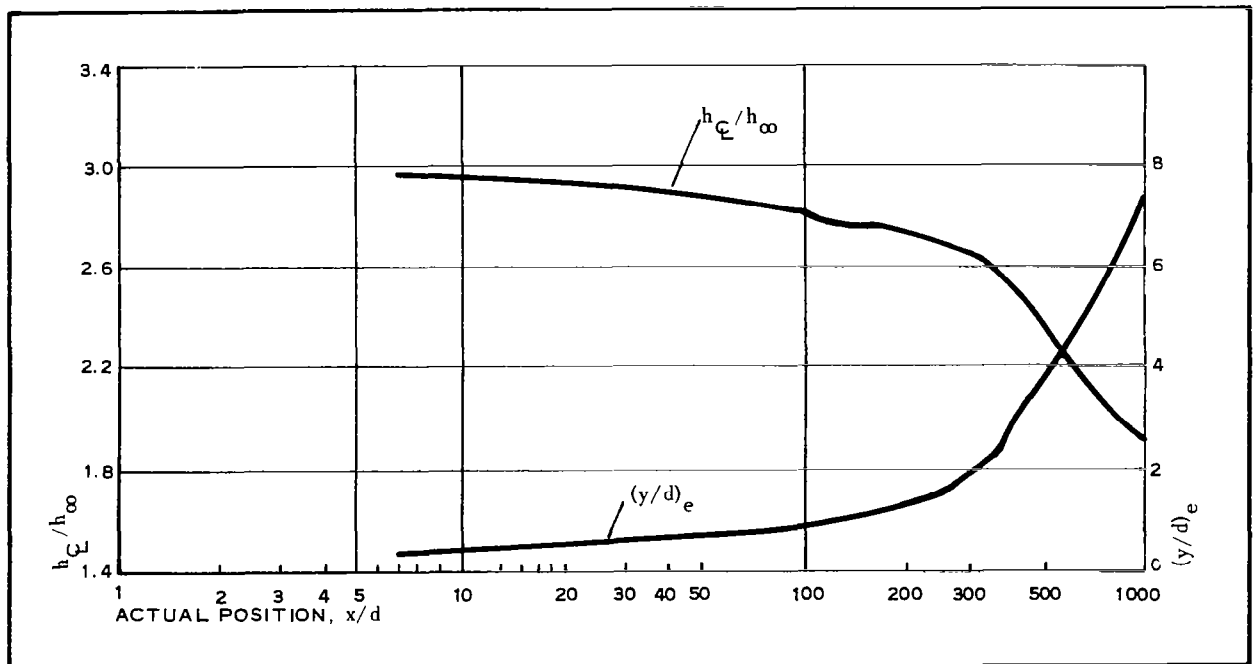


Figure 10 - Theoretical Turbulent Wake Growth

where

$x$  = distance aft of a body,

$u_{\infty}$  = free stream axial velocity,

or

$$\frac{x}{r_n} \approx u_{\infty} r_n \quad \frac{\rho c_p}{k} = \text{RePr} ,$$

where

$\text{Re}$  = Reynolds number,

$\text{Pr}$  = Prandtl number.

Hence, the wake at high altitudes stays laminar over long distances. The process of cooling, however, is faster if the wake is turbulent. Naturally, the tendency to develop turbulence is associated with the region of highest velocity gradients, which is located in the inner wake. The experiments of Demetriades<sup>18</sup> indicate that transition for two-dimensional and axisymmetric flows (wedges and cones) occurs at Reynolds number corresponding to the altitudes of the order of 150,000 ft. The expansion of physical boundaries of the wake is due to a decrease in static pressure and flow expansion. The initial development of the inner wake is a function of the momentum thickness, which is about 10 times smaller than the body diameter. The velocity gradient across the inner wake decays from its maximum at the neck to a value of about  $150 \theta$  ( $\theta$  = momentum thickness) at approximately  $10 \leq x/d \leq 20$ . At this location the momentum defect of the outer (inviscid) wake is swallowed by the inner wake at the rates that cannot be ignored. Initially, eddy diffusivity  $\epsilon_T$  depends on the local drag at the neck. The rate of growth  $d\epsilon_T/dx$  depends on the rate  $d\theta/dx$ , which in turn depends on the  $(\partial h/\partial y)_y = y_e$  and  $dy_e/dx$ . In addition the  $dy_e/dx$  also depends on  $\epsilon_T$ .



The  $(\partial h / \partial y)_y = y_e$  is small at  $y_e/d \ll 1$ ; hence,  $\epsilon_T$  and  $y_e$  (inner wake thickness) increase slowly until the region of inviscid outer wake is reached where  $\partial h / \partial y$  is significant. Then rapid growth in  $\epsilon_T$  and  $y_e$  is expected, which eventually slows down.

Since the flow in outer wake is not affected by the inner wake in the region of  $x/d < 2 - 10$ , the enthalpy is specified by the inviscid flow relations. In addition, the drag contributed by the static pressure is not large (static pressure is about five times ambient) at high altitudes compared to the momentum defect. At  $x/d = 20$  or less, the static pressure is ambient and the flow is frozen or in thermodynamic equilibrium.

In the inner wake it is assumed that turbulence intensity at each  $x/d$  is proportional to the local velocity gradient, and its spread in the  $y$  direction is proportional to the wake width at each  $x/d$ .

At  $x/d > 5$  to  $10$ , the total enthalpy is essentially constant across the inner wake, being equal to the total enthalpy of the inviscid flow.

## 5. WAKE GROWTH

The wake growth is essentially a turbulent process, since the growth itself is a dynamic process that is associated with formation of disturbances. Three important factors determine the growth of the wake: (1) shape variation (blunt versus sharp), (2) effect of shape when bodies have the same drag coefficient, and (3) effect of altitude (Reynolds number).

The conclusions reached by Hromas and Lees indicate the following effects at high velocity:

1. The shape effect on initial core drag is small, since both the sphere and cone of the same base have nearly equal core drag. On the other hand, the size or pressure expressed by the Reynolds number of the body is significant.

2. Although the wake shock can change the shape of the outer (inviscid) profile rather drastically, (especially at a low Mach number) the inner wake is not affected to any degree, since inviscid enthalpy is low.
3. The rates of turbulent growth behind the cones are lower than for the blunt bodies for up to  $x/d \lesssim 10^4$ .
4. Wake enthalpies behind the cones decrease faster by an order of magnitude than behind the spheres.
5. Two bodies of different shape having the same drag coefficient will exhibit different wake histories until the asymptotic conditions are reached somewhere downstream.
6. If the core drag (momentum defect of inner wake) or altitude are increased, the difference in a wake due to the body shape tends to disappear.

The study of Lykoudis<sup>22</sup> indicates the following trends in wake growth:

1. Blunt or slender bodies show higher rates of growth for the turbulent core (present in any wake) as the Mach number and enthalpy are increasing in the neck up to  $x/d \approx 10^2 d$  region. From there on, the growth is as  $[C_D A(x)]^{1/3}$ .
2. Growth is irregular if geometry is so that overexpansions and recompressions are formed.
3. The blunt or slender bodies at the same altitude and Mach number indicate the same order of magnitude for the enthalpy, which decays faster for a cone than a blunted body, although the  $C_{D_{tot}}$  may be equivalent.

Slattery and Clay<sup>23</sup> pointed out that, to the first order, the history of velocity profile can be expressed by the momentum terms.

Hence, by the conservation of momentum, at some  $x/d = n$  downstream:

$$A_{w_n} u_n^2 \rho_n + \frac{1}{2} C_{D_B} A_B \rho_{n-1} V_B^2 = A_{w_n} V_B^2 \rho_{n-1}, \quad (13)$$

where

$A_{w_n}$  = wake area at  $n$  station,

$u_n$  = local wake velocity,

$\rho_n$  = average density at  $n$ ,

$C_{D_B}$  = body drag coefficient,

$A_B$  = body area

$\rho_{n-1}$  = density upstream of  $n$ ,

$V_B$  = body velocity,

and conservation of mass is

$$A_B \rho_{n-1} V = A_{w_n} \rho_n V_w, \quad (14)$$

where wake velocity  $V_w = V_B - u$ .

Then the ratio  $V_w/V$  is

$$\frac{V_w}{V} = \frac{1}{2} C_{D_B} \frac{A_B}{A_{w_n}}, \quad (15)$$

and since  $A_{w_n} = \pi r_w^2$ , the wake growth in the axial direction is inversely proportional to the square of its radial growth as indicated in Figure 11. However, two bodies of different shape, but with the same drag coefficient at the same time, position, and velocity may not exhibit the same

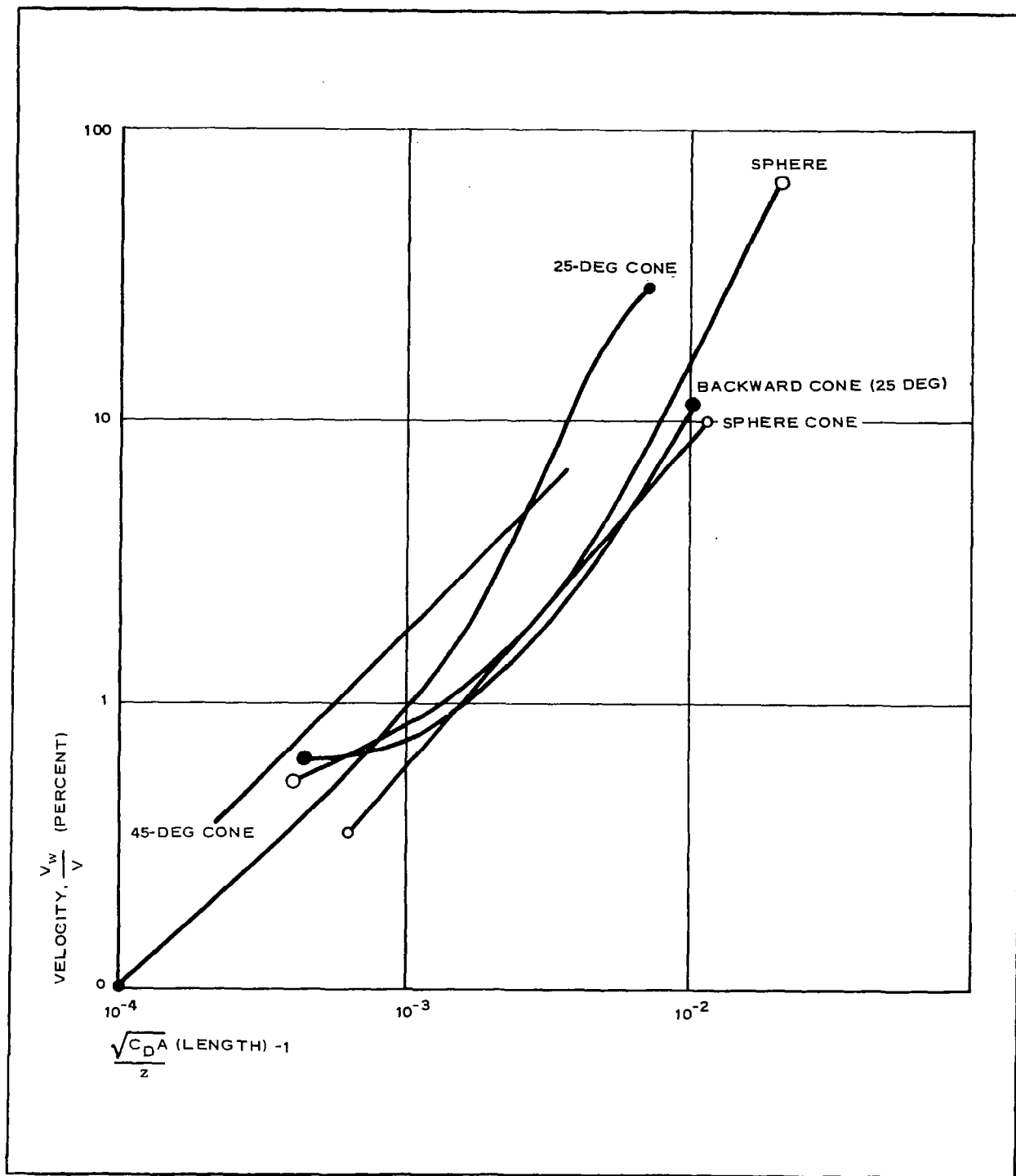


Figure 11 - Velocity Defect in Wake<sup>22</sup>

wake shape as shown in Figure 12 (spherical cone versus 45-deg cone), and this means that they do not have the same wake velocity at a given  $x/d$ .

In this particular case, the wake behind the 45-deg cone is narrower (or has less mass); hence the local velocity is greater. The behavior also may be described by the conditions of thermodynamic equilibrium, which depends on the enthalpy in the axial direction in the inner wake and the radial enthalpy gradient in the outer (inviscid) wake (Lees<sup>17</sup>).

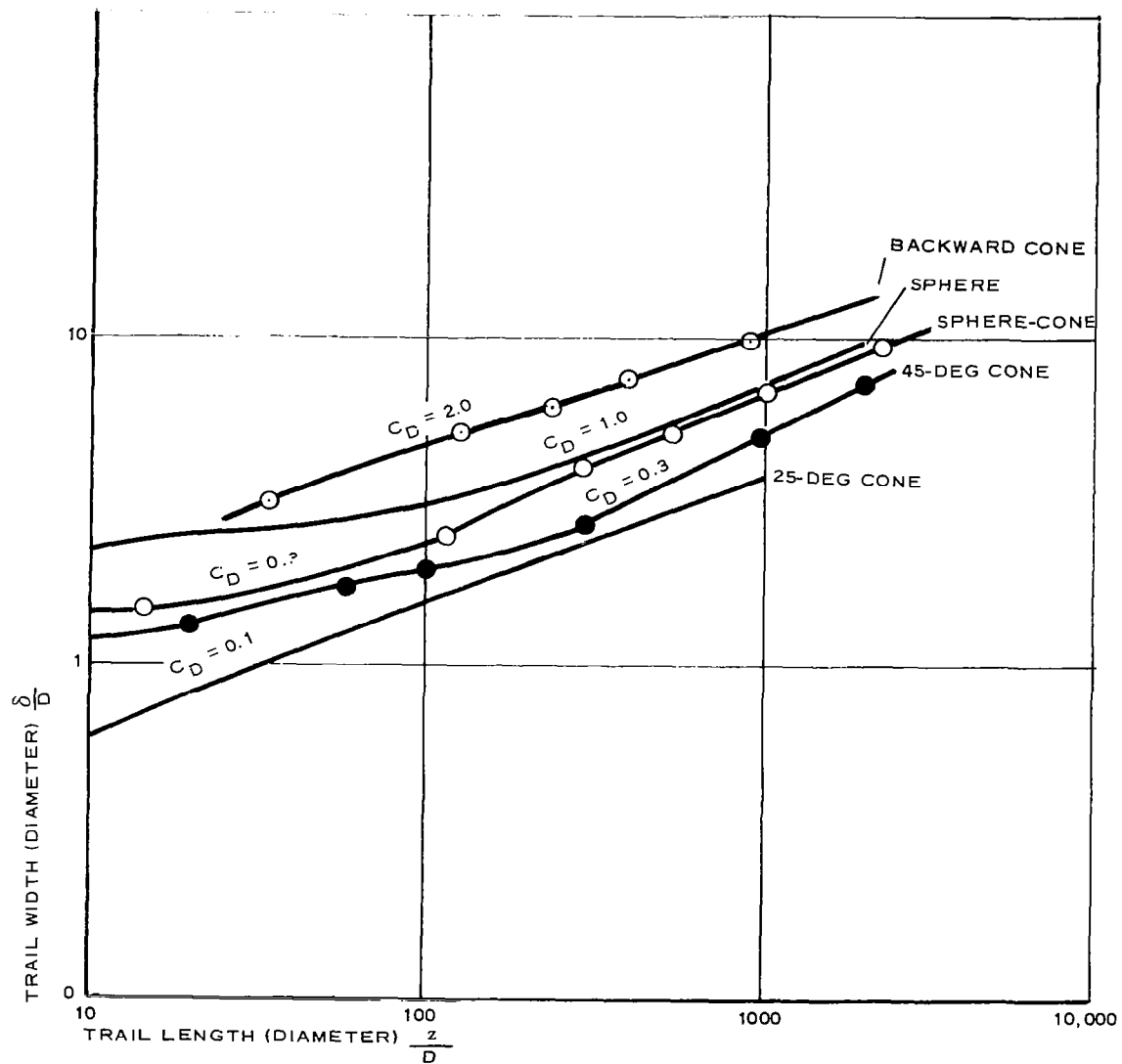


Figure 12 - Trail Width versus Trail Length for Various Bodies  
( $V \approx 7000$  FPS)<sup>22</sup>



## SECTION IV - PREDICTION OF THE WAKE QUALITIES

### 1. GENERAL

The analysis of wakes consists of the theoretical prediction, observations, measurements, and correlation of empirical data. Like in any branch of science for a postulate or hypothesis to become a theory, the experimental evidence must confirm the theoretical relationships.

Prediction of aerodynamic wakes is as yet inadequate, since the proposed theoretical models are not fully confirmed by the observations and measurements. The available wind tunnel and ballistic range data provide limited confirmations for the pure wakes (Lees and Hromas<sup>21</sup>). The major obstacle remaining is to obtain reliable and detailed data. The problem is especially acute for the wake modified by the presence of the trailing decelerator. The approaches, the methods to verify them and the quality of data obtained are varied, uncoordinated, and unsystematic; thus, they are described as attempts.

### 2. THEORETICAL ATTEMPTS

There is a number of proposed solutions, some of them classical (Blasius, Thomson, Goldstein, etc.), the others of a more applied nature. All are essentially the attempts to fit the solutions, obtained from the available mathematical techniques, to the physical phenomena of diverse and complicated nature. The equations governing these phenomena were derived many years ago in the appropriate set of coordinates (cylindrical mostly with some applications in cartesian or spherical) and are:

1. Navier-Stokes equations
2. Equation of continuity



### 3. Equation of state

### 4. Equation of energy conservation

The interpretation and solution of equations is another matter. The main difficulty is their nonlinearity. However, a number of particular solutions are available for a limited number of the boundary conditions (Schlichting and others).

The other solutions are of the so-called similar nature or are simply the mathematical treatments describing a phenomenon similar to one for which exact solution is not possible (Falkner-Skan solution).

These other solution treatments are:

1. Laminar near wake of blunt bodies in hypersonic flow (Lees and Reeves<sup>24</sup>) solution, which is characterized by joining the two regions (base and near wake) by a set of conditions and a singular point (at neck). The viscous interaction is treated by the moment-integral method.
2. Second order solution for the velocity distribution in turbulent wake (Heinrich and Rust<sup>25</sup>) which is an approximation to solve the incompressible turbulent wake.
3. Presentation of entropy wake, diffusion wake, and simplified wake models with compressibility and shear accounted for by the simplified approximate solutions (Goulard<sup>26</sup>).
4. Wake behind blunt bodies method, where finite difference technique solves the viscous wake, and one-dimensional compressible flow equations account for the inviscid part (Zeiberg, Bleich<sup>27</sup>).

5. Fluid mechanics of wakes in hypersonic flow in transformed and physical plane (Ting, Libby<sup>28</sup>).
6. Similar solutions for axisymmetric incompressible wakes based on Falkner-Skan equation (Kubota, Reeves<sup>29</sup>).
7. Attempt to treat the three-dimensionality in viscous wakes (Steiger, Bloom<sup>30</sup>), and also two-dimensional asymmetric wakes.<sup>31</sup>
8. Treatment of the nonequilibrium laminar wake by the finite difference method (Zeiberg and Bleich<sup>27</sup>).
9. The solution of the two-dimensional laminar wake for the arbitrary shape body by the integral method (Korkan<sup>32</sup>). It is vague concerning the near wake and the neck region but may be indicative for the conditions prevailing there. The integral method is based upon the Dorodnizyn transformation and assumption that closed polynomial represented by the four terms can form an approximation for the velocity and enthalpy profiles if the boundary conditions at the center line and the edge can be satisfied.
10. The evaluation of the wake parameters when the decelerator of the Ballute<sup>a</sup> type is present in the wake is made by making an assumption that at  $x/d \gtrsim 6$ , the wake has a cylindrical, constant width, and shape due to the presence of a riser line that holds the wake-centerline velocity at zero (Nerem<sup>33</sup>). Otherwise, the approach is identical to that found in

---

<sup>a</sup>TM, Goodyear Aerospace Corporation, Akron, Ohio. 44315

Reference 32. It is more limited, however, since it assumes the starting point downstream of the neck. The presence of the "cylindrical wake" in the absence of the detail information is a postulated statement.

11. Approximate solution for the inviscid wake behind a blunt body at hypersonic speed is based on the balance of the mass flow in the free stream going through the shock to that behind the shock, all included in the control volume bounded by the imaginary disks (Nerem<sup>34</sup>).
12. The particle-in-cell method to obtain time-dependent development of the plane or cylindrical wake behind the flat base of a body moving at supersonic speed (Amsden, Harlow<sup>35</sup>) based on the numerical technique, which for this investigation neglects the viscous and real gas effects.

### 3. EXPERIMENTAL ATTEMPTS

The experimental measurements of the wake parameters are usually performed in the wind tunnels and ballistic ranges. The models mounted on the various rigid supports or fired down the range are usually well-defined two-dimensional or axisymmetric bodies (sphere, cone, spherical cylinder, or a combination). The data are taken by the pitot-and-static pressure probes, hot-wire techniques and/or schlieren photography.

The following typical examples are listed:

1. Pitot and static pressure measurements in the wake of the cone-cylinder at  $M_{\infty} = 2.30$  and  $4.65$ . They cover the base region and the near wake ( $0.21 \leq x/d \leq 7.56$ ). With careful interpretations, the data

can be useful in determining flow environment in the wake (McShera<sup>36</sup>).

2. Stagnation temperature fields behind a 10-deg, half-angle wedge and cone (Todisco and Pallone<sup>37</sup>) are given at  $M = 16$ . Data are useful for the temperature predictions in the near wake.
3. Complete study of wakes behind the circular cylinder at  $M = 5.7$  (McCarthy and Kubota<sup>38</sup>) is the good example of the wake study.
4. Another rather complete study of the near wakes behind a two-dimensional cylinder at  $M_{\infty} = 18, 19, 21$  and  $2 \leq x/d \leq 8$  is given in Brown, Kramer, Smith.<sup>9</sup>

The separate class of the wind tunnel data deals with the evaluation of the aerodynamic deployable decelerators placed behind the primary bodies. Unfortunately, it is limited to the drag measurements (drag coefficients), and therefore only the gross effects of the wake environment are indicated. The data can be summarized along the parameters given in Table I. For details consult References 39 to 50.

It is noted here that Table I presents the summary for the aerodynamic decelerator performance in a wake of a particular payload in terms of the drag coefficient, drag efficiency, pressure distributions, and stability whenever available. The data are representative and indicative, but must be used with mature judgment since the wind tunnels, test purposes, and models are rather heterogeneous in nature. Interpretation of the given results requires the knowledge of the fluid mechanics, including viscosity and compressibility.

Hence, the drag coefficients that depend on the Mach number and Reynolds numbers, generally being higher at lower similarity parameter magnitudes ( $M$ ,  $Re$ ), are modified by the viscous flow effects in a wake. The

viscosity effects are more pronounced at the lower  $x/d$  ratios, but can be modified by the decelerator shape, size, and the mode of connection with a primary body.

TABLE I - AERODYNAMIC DECELERATOR PERFORMANCE IN A WAKE

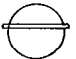


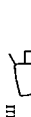







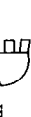







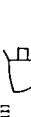





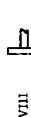
Decelerator configuration	Payload configuration	$M_\infty$	$Re_{ft}$	$\frac{x}{d_B}$	$\frac{d_D}{d_B}$	$C_D$		$\frac{C_{Dw}}{C_{Dp}} = \frac{w}{p}$	$C_p$	Stability	Remarks
						Minimum	Maximum				
Spheres 	I 	2 to 4.65	0.78 to $1.17 \times 10^6$	2 to 12	0.55 to 5.0	0.56	0.90	No	No	Fair to good	Stability comments are limited. TN D-1785 (Reference 39)
	II 	2 to 4.65		2 to 12		0.53	0.88	No	No	Fair to good	
	III 	2 to 4.65		2 to 12		0.50	0.80	No	No	Fair to good	
Cones (right) 60 deg 90 deg 	I 	1.57 to 4.65	3 to $6 \times 10^6$	2 to 6	0.88 to 2.05	0.36	0.90	No	No	Variable	With and without connector. TN D-9794 (Reference 40)
	II 	1.57 to 4.65		2 to 6		0.38	0.80	No	No	Variable	
	IV 	1.57 to 4.65		2 to 6		0.27	0.90	No	No	Variable	
	I 	1.57 to 4.65		2 to 12		0.52	0.85	No	No	Variable	
Conical rings 	II 	1.57 to 4.65	0.70 to $1.18 \times 10^6$	2 to 12	0.89 to 2.05	0.52	0.76	No	No	Variable	TN D-1789
	III 	1.57 to 4.65		2 to 12		0.36	0.62	No	No	Variable	
	I 	2.0 to 4.65		2 to 6		0.82	1.38	No	No	Good	
80-deg modified cone 	II 	2.0 to 4.65	$1.78$ to $3.24 \times 10^6$	2 to 6	0.89 to 2.05	0.76	1.30	No	No	Good	TN D-1789
	I 	2.0 to 4.65		2 to 6		0.82	1.38	No	No	Good	
	I 	2 to 2.87		2 to 12		0.58	0.98	No	No	Variable	
60-deg modified cone 	II 	2 to 2.87	0.70 to $1.17 \times 10^6$	2 to 12	0.89 to 2.05	0.63	0.88	No	No	Variable	TN D-1789
	III 	2 to 2.87		2 to 12		0.42	0.82	No	No	Variable	
	I 	1.47 to 2.5		1.25 to 3.0		0.42	0.81	No	Yes	Not available	
Spheroid (balloon) 	V 	1.47 to 2.5	0.55 to $1.0 \times 10^6$	1.25 to 3.0	1.25 to 3.00	0.38	0.81	No	Yes	Not available	Connector: telescoping tube (actuator). With and without fence $T_c = f(\theta)$ also given TN D-919 (Reference 41) Rigid models
	VI 	1.47 to 2.5		1.25 to 3.0		0.47	0.90	No	Yes	Not available	
	VII 	1.47 to 2.5		1.25 to 3.0		0.40	0.84	No	Yes	Not available	
	VIII 	1.47 to 2.5		1.25 to 3.0		0.40	0.84	No	Yes	Not available	

TABLE I - AERODYNAMIC DECELERATOR PERFORMANCE (Continued)



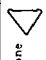



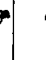



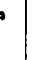









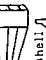



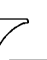

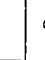

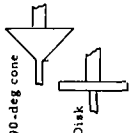
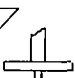

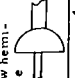
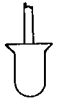
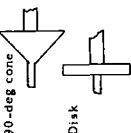
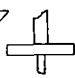
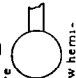
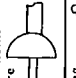
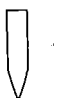

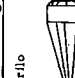



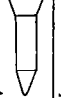
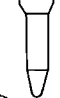
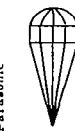
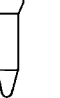
Decelerator configuration	Payload configuration	$M_\infty$	$Re_{ft}$	$\frac{x}{d_B}$	$\frac{d_D}{d_B}$	$C_D$ Minimum Maximum	$\frac{C_{D_w}}{\eta^2 C_{D_\infty}}$	$C_P$	Stability	Remarks
 Spheroid		2 to 4.65	$0.67 \text{ to } 1.09 \times 10^6$	0.5 to 11.9	3.36	0.8	No	No	Variable	TN D-1601 (Reference 42), inflatable
 80-deg cone		2 to 4.65	$0.67 \text{ to } 1.3 \times 10^6$	1.0 to 13.0	2.94	0.93	No	No	Good	TN D-1601, inflatable
 80-deg Ballute		2.5 to 4.65	$1.15 \text{ to } 2.24 \times 10^6$	2 to 9	3.36	0.78	No	No	Good	TN D-1601, inflatable
 80-deg Ballute		10.0	$0.36 \text{ to } 1.8 \times 10^6$	9 to 18	3.3 to 5	0.35	No	Yes	Good	Connector: 0.094-in. cable h is given Models: rigid and inflatable AFSC: TDR-62-39 (Reference 56)
 80-deg Ballute		4.65	$1.6 \times 10^6$	0 to 10.5	0.75	0.02	No	No	Not available	
 80-deg Ballute		4.65	$1.6 \times 10^6$	0 to 10.5	1.24 to 2.47	0.20	No	No	Not available	
 Hyperflo		4.65	$1.6 \times 10^6$	0 to 10.5	0.875	0.08	No	No	Not available	NASA data behind X-15 NASA TN D-3285 (Reference 50)
 Tension shell		4.65	$1.6 \times 10^6$	0 to 10.5	1.00	0.10	No	No	Not available	
 Cone		4.65	$1.6 \times 10^6$	0 to 10.5	1.00	0.05	No	No	Not available	
 80-deg Ballute		1.5 to 6.0	$0.91 \text{ to } 2.35 \times 10^6$	6 to 12	3.75	No	No	Yes	Not available	$C_P = f(y/R, x/d, M)$ Models: rigid AFSC: TDR-64-65 (Reference 43)
 90-deg cone		0.85 to 1.25	$3.1 \text{ to } 3.4 \times 10^5$	2 to 8	1.00	0.20	Yes	No	Not available	
 Disk		0.85 to 1.25	$3.1 \text{ to } 3.4 \times 10^5$	2 to 8	2.00	1.04	Yes	No	Not available	
 Sphere		0.85 to 1.25	$3.1 \text{ to } 3.4 \times 10^5$	2 to 8	1.00	0.20	Yes	No	Not available	RTD-TDR-63-4242 (Reference 46)
 Hollow hemi-sphere		0.85 to 1.25	$3.1 \text{ to } 3.4 \times 10^5$	2 to 8	2.00	0.38	Yes	No	Not available	
					1.00	0.21	Yes	No	Not available	
					2.00	0.8	1.32			

TABLE I - AERODYNAMIC DECELERATOR PERFORMANCE (Continued)

Decelerator configuration	Payload configuration	$M_\infty$	$\frac{R_e}{R}$	$\frac{\lambda}{d_B}$	$\frac{d_D}{d_B}$	$C_D$		$\eta' = \frac{C_{Dw}}{C_{D\infty}}$	$C_F$	Stability	Remarks
						Minimum	Maximum				
 90-deg cone  Disk  Sphere  Hollow hemisphere	 IV	4.35	$3.0 \times 10^5$	2 to 8	2.00	0.19	0.45	Yes	No	Not available	RTD-TDR-63-4242
		4.35	$3.0 \times 10^5$	2 to 8	1.00	0.07	0.31		No	Not available	
		4.35	$3.0 \times 10^5$	2 to 8	2.00	0.19	0.28	Yes	No	Not available	
		4.35	$3.0 \times 10^5$	2 to 8	1.00	0.05	0.33		No	Not available	
 90-deg cone  Disk  Sphere  Hollow hemisphere	 XII	4.35	$3.0 \times 10^5$	2 to 8	2.00	0.26	0.62	Yes	No	Not available	RTD-TDR-63-4242
		4.35	$3.0 \times 10^5$	2 to 8	1.00	0.20	0.88		No	Not available	
		4.35	$3.0 \times 10^5$	2 to 8	2.00	0.34	0.46	Yes	No	Not available	
		4.35	$3.0 \times 10^5$	2 to 8	1.00	0.16	0.51		No	Not available	
 80-deg Ballute  Hyperflo  Parasitic	 XIII  I  XIV  XV	2 to 4	$0.91$ to $1.54 \times 10^6$	2 to 3	1.24	0.30	1.05	Yes	No	Not available	Connector: (Int AEDC-TR-65-218 (Reference 57))
		2 to 5.5	$4.15$ to $9.3 \times 10^5$	7 to 11	0.95	0.23	1.03	No	No	Marginal	AFFDL-TR-65-150 (Reference 49)
		4 to 5.5	$6$ to $9 \times 10^5$	5 to 9	$\approx 0.90$	0.41	0.65	No	No	Marginal	AEDC-TR-65-57 (Reference 59)
		2.6	...	7.16	2.55	0.51		No	No	Good	AEDC-TDR-64-120 (Reference 58)
 Parasitic	 XV	2.2	...	9.75	2.55	0.53		No	No	Good	AEDC-TR-65-57 (Reference 59)
		2.6 to 3.0	...	12.57	2.55	0.41	0.53	No	No	Good	





## SECTION V - DECELERATOR IN THE WAKE

The aerodynamic deployable decelerator is attached to the payload in such a manner that the drag force generated is along the line of motion for the best efficiency of the overall force-moment diagram at any given time. Such an orientation places the decelerator in a flow region that consists totally or partially of the wake flow of the payload in general. In particular, the decelerator, at least theoretically, can be placed (depending on the deceleration-stabilization requirements, mass-volume ratios and geometrical proportions) in the following flow regions: the base flow or near-to-medium wake flow ( $2 \leq x/d \leq 15$ ) in the axial direction. In the lateral direction, the decelerator can operate in the following flow regions:

1. Viscous inner wake
2. Viscous inner wake and inviscid outer wake
3. Viscous wake, inviscid outer wake, shock layer(s) and free stream

Generally, the problem of evaluation of a decelerator is essentially not different from any problem of a body in the flow, provided the flow properties are known. However, in this case the wake flow has specific complicated properties. In addition, the relatively close proximity to the body creating the wake, plus the fact that the body and decelerator are connected by a means subject to the laws of rigid mechanics, introduces complexities that require a more rigorous analysis. The near wake for low Mach numbers ( $M_{\infty} \ll 1$ ) forms vortexes and is unsteady over a wide range of Reynolds numbers. Since the Reynolds number is low and streamwise changes are not small compared with those in the normal direction, the boundary layer approach is not adequate. In addition, at low Reynolds numbers the flow is unstable (or turbulent); hence there is no laminar flow when the Reynolds

number becomes large. If the flat plate assumption is feasible, then the laminar boundary layer solution may be applicable.

The near wake for  $M_\infty > 1$  or more rigorously for  $M_\infty \gg 1$ , forms an annulus by free shear layers that converge to a neck (the rear stagnation point) from which it expands downstream. For the blunt payloads, the local Mach number adjacent to the shear layer becomes frozen at  $M_L \approx 3.0$ , but for the slender payloads the same Mach number approaches the free stream value, i.e.,  $M_L \rightarrow M_\infty$  due to the body shock wave configuration. Investigations of Lin,<sup>51</sup> and Chapman, et al.,<sup>52</sup> indicate that at supersonic external Mach numbers the stability of a laminar shear layer increases markedly as the Mach number increases. This is carried over into the neck region; thus, the portion of the inner wake will be also laminar over a range of Reynolds numbers, as noticed by Lees and McCarthy. The stable nature of the flow over a particular range of  $(x/d)$ 's will provide a favorable environment for the steady pressure and velocity distribution in the same range of  $(x/d)$ 's. It appears as a constant region on the two-dimensional flow diagram which transforms into laminar waves in the viscous wake, triggering the transition.

The trend described above is confirmed by the plots of Figures 13 and 14, which are based on experimental data. The data of Figure 13 indicate the local flow conditions immediately ahead of the decelerator's vertex. Figure 14 illustrates the trend in terms of the drag coefficient. The existence of stability region and its boundaries are strongly dependent on subsonic, sonic, and supersonic disturbances, which are due to perturbances, vorticity, compressibility, and temperature of the fluid. The influence of connectors, riser lines, etc., can be either stabilizing or destabilizing, depending on their size, configuration and the local flow.

The intelligent evaluation of the decelerator flow field requires the knowledge of such parameters as local Mach numbers, pressures, densities, and temperatures. The verification of the suggested theoretical wake models by experiment is the goal that has not yet been attained. Thus, the interaction is described at best in hypothetical terms. If interaction is approached by the

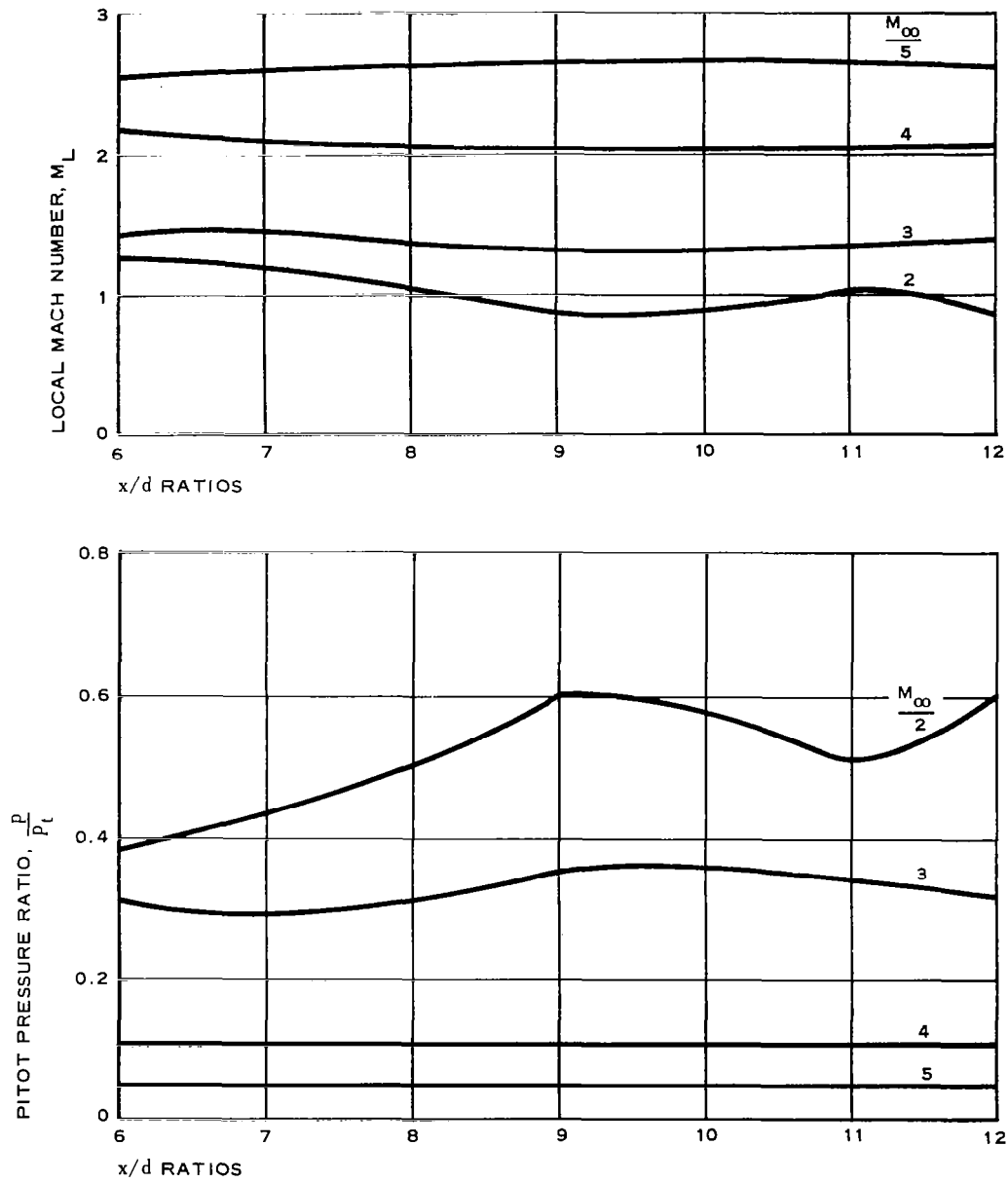


Figure 13 - Local Flow Conditions in a Wake of a Missile in the Presence of the Ballute Decelerator<sup>53</sup>

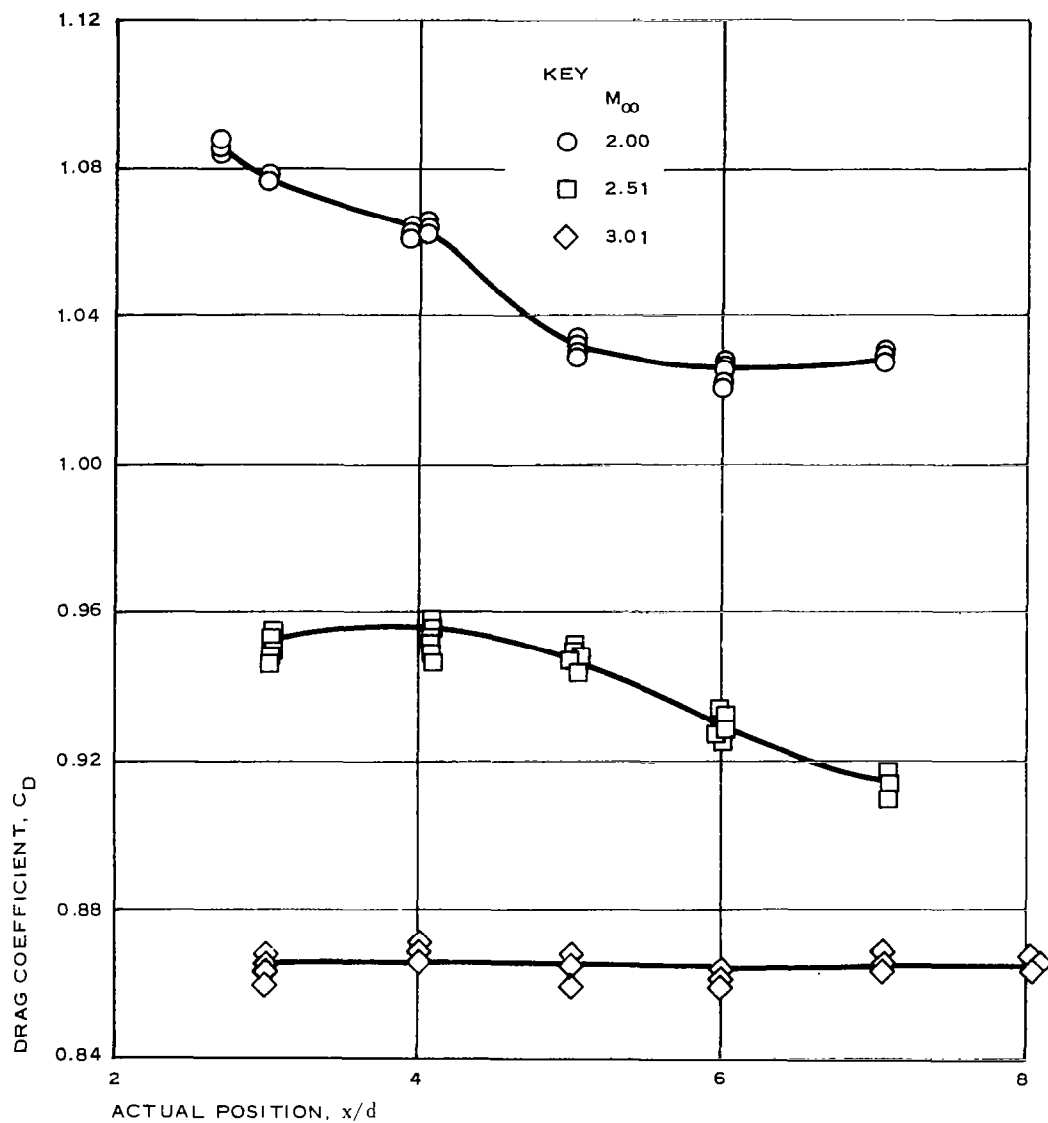


Figure 14 - Variation of Ballute Drag Coefficient with Payload-Ballute Separation Distance<sup>53</sup>

principle of the momentum defect, then one can postulate that, knowing initial conditions at the forebody base, the growth of the wake depends on the momentum transport in the wake with skin friction of connector and riser lines contributing to the local profiles.

Prandtl's concept of viscous flow and the assumption that local acceleration in the inner wake is more pronounced than acceleration due to external pressure gradient allow the following expression for the momentum integral equation:

$$\rho_1 u_1^2 (\pi \theta_1^2) = 2\pi \int_0^\delta \rho u (u_1 - u) r dr = C_x, \quad (16)$$

where

$\theta$  = momentum thickness,

$\delta$  = wake thickness,

$r$  = radial coordinate,

$u$  = velocity in x-direction,

$C_x$  = constant with respect to  $x$ , and

$l$  = wake edge.

To satisfy the conservation of momentum,

$$\rho_B u_B^2 (\pi \theta_B^2) = \rho_1 u_1^2 (\pi \theta_1^2), \quad (17)$$

where B refers to conditions at the base and  $d$  is body diameter.

If the above postulate is true, then at certain  $x/d$  locations and constant Mach number, a particular decelerator configuration will exhibit only slight variations in drag coefficient. Considering Figure 15 as representative, this concept is apparently valid for

$$2 \leq M_\infty \leq 4 \text{ at } 7 \leq x/d \leq 11$$

and for

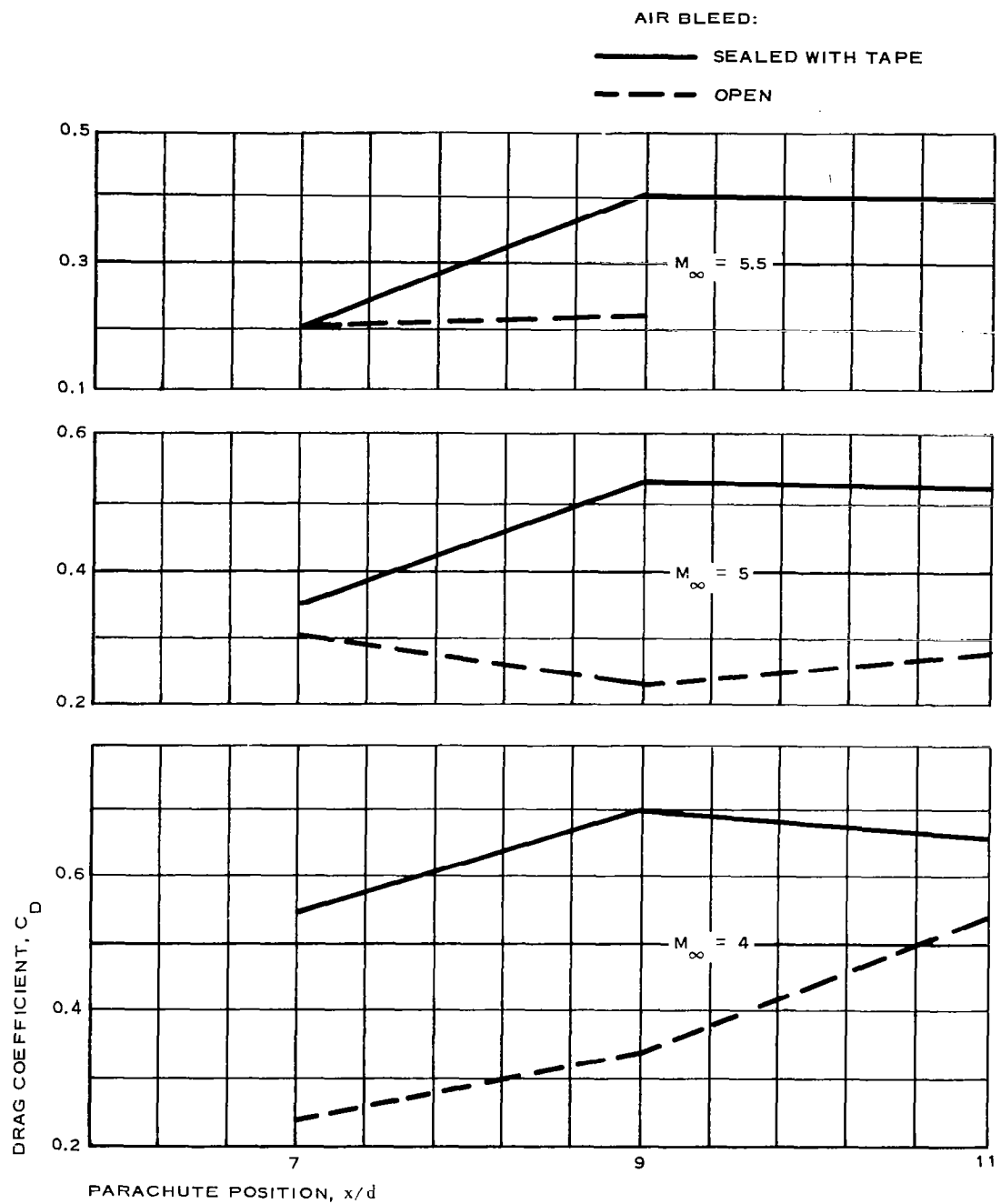


Figure 15 - Effect of Air Bleed on Parachute, Model 20 behind Forebody Type II<sup>49</sup>

$$M_{\infty} = 5 \text{ to } 5.5 \text{ at } x/d = 9 \text{ to } 11 .$$

Figure 16 shows the influence of the forebody configuration on the momentum defect for the same Hyperflo configuration that would be expected. Figure 17 indicates the expected Mach number influence.

In considering the interference phenomena, the following areas of the flow analysis should not be overlooked:

1. Shock wave-wake edge interaction and its influence on the wake width
2. Shock wave-boundary layer interaction propagated downstream
3. Formation of separated flow due to the presence of riser lines leading to drag reduction of a decelerator
4. Base pressure values and their influence on the drag of decelerators
5. Formation of the new boundary layer by the part of a shear layer that negotiates the pressure rise at the neck and forms a new uniform stream with the redeveloped boundary layer
6. Decrease of mixing coefficient with increasing Mach number and consequently little mixing at the base that affects the wake



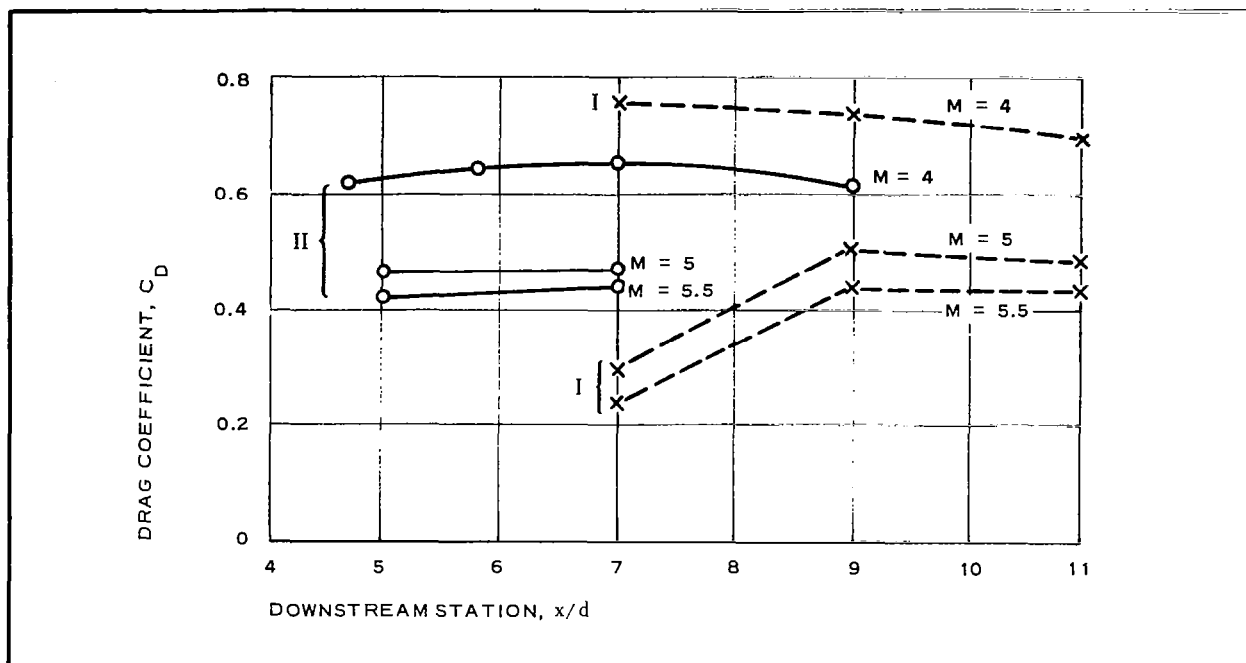


Figure 16 - Drag versus  $x/d$ , Hyperflo Model 1 behind Type I and II Forebodies<sup>49</sup>

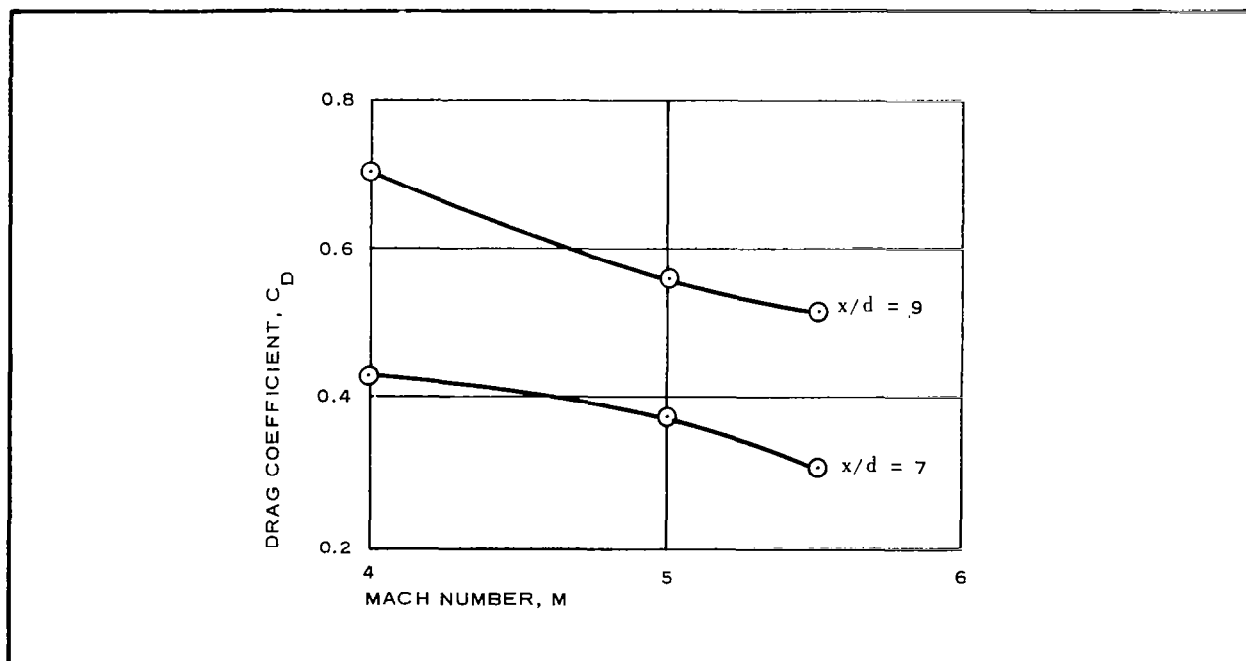


Figure 17 - Drag versus Mach Number, Hyperflo Model 2 behind Forebody Type I<sup>49</sup>

## SECTION VI - CONCLUSIONS AND RECOMMENDATIONS FOR FUTURE WORK

The problems of flow analysis behind bodies in motion have received considerable attention during the past several years. Out of necessity, the recent investigations (both theoretical and experimental) are dedicated to the hypersonic velocity regime and are based on the basic, classical works of fluid mechanics that were performed with either incompressible or idealized fluids. What is noted, however, is the rather superficial treatment of the wakes in transonic and supersonic flow regimes, which at this stage of development of the deceleration systems, are of great importance.

The basic obstacles in solving the wake problem at any speed regime are the uncertainties in application of the well-established asymptotic techniques of fluid mechanics.<sup>54</sup> Hence, all theoretical attempts using asymptotic techniques that are strictly valid either for very small or very large Reynolds numbers exclude the enthalpic and entropic considerations, as well as the influence of viscous forces. Specifically, the following conclusions are reached concerning the general theory of wakes:

1. There is no complete theory of near wake accounting for the base flow, circulation, base heating, and other elements.
2. Several shear layer solutions available are incomplete to be considered as a near wake solution, and thus are questionable with regard to relating the nonequilibrium boundary layer solution at shoulder to the flow at the rear stagnation point (the region of the wake neck).
3. Prediction of transition point  $X_{Tr}$  is a matter of

extrapolation of small-scale laboratory data to the full-scale flight conditions.

4. The choice of scaling parameters is not obvious but can have considerable effect.
5. Uncertainties in understanding the physical mechanism of turbulent flow are still sizeable.
6. Hypersonic near wake experiments indicate that the Mach number has little effect on the position of the rear stagnation point but rather strong effect on location of the neck.<sup>55</sup>

The area of investigation of wake influence upon the aerodynamic decelerators finds itself in a rudimentary stage, consisting mainly of some experimental data that indicate the drag efficiency and stability of a particular decelerator behind a particular payload. These data in a concise form are presented in Table I. The table encompasses all published (unclassified) information between the 1960-to-1965 period and gives the scope, main parameters, and representative values for the configuration investigated.

The progress in wake investigations undoubtedly has been made but more systematic studies are needed. And since the problem of pure wake is coupled with the problem of its influence upon the decelerator both of them should move in parallel if not in series. Moreover, it is felt that before the "new" theories are proposed and new sets of academic data are computed, the existing postulates should be checked and systematic careful experiments should be run in the near wake of the laminar, transitional, and turbulent regimes such that average local properties (pressures, temperatures, velocities, electro-chemical processes) are obtained for the basic configurations already investigated. In addition, the fluctuations and valid correlations are needed not only for the prediction of data but also for the data already existing, which are often uninterpreted or misinterpreted. In other words, scientific breakthrough cannot be achieved by the "right hit" but requires a systematic "stepping-stone" effort.

## LIST OF SYMBOLS

$A$  = constant

$A_B$  = body reference area

$A_w$  = wake cross-sectional area at station  $n$

$c$  = Chapman-Rubesin parameter

$C_{D_{tot}}$  =  $D_{tot}/qA$ , total drag coefficient

$C_{D_f}$  = boundary layer drag coefficient

$C_{D_p}$  = pressure drag coefficient

$C_{D_w}$  = drag coefficient in wake

$C_{D_B}$  = body drag coefficient

$C_{D_\infty}$  = drag coefficient in free stream

$c_f$  = skin friction coefficient

$c_p$  = specific heat

$C(k)$  = mixing rate correlation function

$C_x$  = constant with respect to  $x$

$d$  = body diameter

$H$  = total enthalpy  
 $h$  = static enthalpy  
 $j$  = power index  
 $k$  = heat conductivity  
 $\ell$  = distance along shear layer  
 $M$  = Mach number  
 $M_L$  = local Mach number  
 $n$  = wake station  
 $P$  = pressure  
 $Pr$  = Prandtl number  
 $Re = V\rho/\mu$ , Reynolds number/foot  
 $r$  = normal coordinate or radius  
 $r_n$  = nose radius  
 $S^*$  = distance coordinate  
 $S$  = shape parameter  
 $T_o$  = temperature (stagnation)  
 $t$  = time  
 $U, u$  = wake velocity in axial (x) direction  
 $U_\infty$  = free-stream axial velocity  
 $V_B$  = body velocity  
 $V_w = V_B - u$ , wake velocity

$w = 1 - u/u_e$ , velocity defect

$x$  = axial distance

$X_o$  = sticking distance

$X_{Tr}$  = transition distance

$y$  = vertical distance

$\bar{y}$  = length normal to wake centerline, transformed

$z$  = wake length

$\bar{x} = \int_0^x \frac{\rho_e \mu_e u_e}{\rho_\infty \mu_\infty u_\infty} \frac{dx}{d} ,$  transformed length measured from neck

$\gamma$  = ratio of specific heats

$\delta$  = wake thickness

$\epsilon_T$  = turbulent body diffusivity

$\eta$  = transformed independent variable

$\eta'$  = drag efficiency

$\theta = 2 \int_0^\infty \frac{\rho u}{\rho_e u_e} (1 - \frac{u}{u_e}) dy,$  momentum thickness

$\mu$  = absolute viscosity

$\rho$  = density

$\sigma = c_p u/k$ , Prandtl number

$\psi$  = streamline

#### Subscripts and Superscripts for Pressure (P)

$( )_P$  = pitot

$( )_b$  = base

$( )$  = static

$( )_e$  = at shear layer outer edge

$( )_l$  = at wake's edge

$P_o$  = stagnation pressure

#### For Mach Number (M)

$( )_\infty$  = free stream

$( )_L$  = local

$( )^*$  = along dividing streamline

#### For Wake Thickness ( $\delta$ )

$( )_w$  = initial

$( )_B$  = at separation

#### For Density ( $\rho$ )

$( )_e$  = wake's edge

$( )_n$  = at station n

$( )_{n-1}$  = upstream of n

#### For Momentum Thickness ( $\theta$ )

$( )_o$  = initial

$( )_s$  = stagnation

#### For Body Diameter

$d_D$  = decelerator diameter

$d_B$  = body diameter

## LIST OF REFERENCES

1. Chapman, D. R. : Laminar Mixing of A Compressible Fluid. NACA TN-1800, February 1949.
2. Baum, E. ; King, H. ; and Denison, M. : Recent Studies of the Laminar Base Flow Region. AIAA 64-5, Electro-Optical Systems, January 1964.
3. Denison, M. ; and Baum, E. : "Compressible Free Shear Layer with Finite Initial Thickness," AIAA Journal, Vol 1, No. 2, February 1963.
4. Kennedy, E. D. : "Wake-Like Solutions of the Laminar Boundary-Layer Equations," AIAA Journal, Vol 2, No. 2, p 225, February 1964.
5. Kubota, T. ; and Dewey, C. : "Momentum Integral Methods for the Laminar Free Shear Layer," AIAA Journal, Vol 2, No. 4, p 625, April 1964.
6. Crocco, L. ; and Lees, L. : "A Mixing Theory for the Interaction between Dissipative Flows and Nearly Isentropic Streams," IAS Journal, Vol 19, No. 10, October 1952.
7. Glick, H. : "Modified Crocco-Lees Mixing Theory for Supersonic Separated and Reattaching Flows," IAS Journal, Vol 29, No. 10, p 1238, October 1962.
8. McCarthy, J., Jr. : Hypersonic Wakes, Graduate Aeronautics Laboratory California Institute of Technology (GALCIT), Memo No. 67, July 1962.
9. Brown, A. ; Kramer, R. ; and Smith, C. : Hypersonic Cylinder Wake Studies at Mach 20, RR-9-63-14, Lockheed Co., September 1963.
10. Hromas, L. ; and Lees, L. : Effect of Nose Bluntness on the Turbulent Hypersonic Wake, Space Technology Laboratories (STL), BSD-TDR62-354, October 1962.
11. Dewey, C. F. : "Near Wake of a Blunt Body at Hypersonic Speeds," AIAA Journal, Vol 3, No. 6, p 1001, June 1965.
12. Pallone, A. ; Erdos, J. ; and Eckerman, J. : "Hypersonic Laminar Wakes and Transition Studies," AIAA Journal, Vol 2, No. 5, May 1964.



13. Gold, H.: Laminar Wake with Streamwise Pressure Gradient for Arbitrary Initial Velocity and Enthalpy Distributions, GALCIT, May 1962.
14. Van Driest, E.; and Blumer, C.: "Boundary Layer Transition: Free-stream Turbulence and Pressure Gradient Effects," AIAA Journal, Vol 1, No. 6, June 1963.
15. Menkes, J.: Comment on "Measured Transition from Laminar to Turbulent Flow and Subsequent Growth of Turbulent Wakes," AIAA Journal, Vol 3, No. 11, November 1965.
16. Slattery, R. E.; and Clay, W. G.: "Reply by Authors to J. Menkes," AIAA Journal, Vol 3, No. 11, November 1965.
17. Lees, L.: "Hypersonic Wakes and Trails," AIAA Journal, Vol 2, No. 3, March 1964.
18. Demetriades, A.: "Hot-Wire Measurements in the Hypersonic Wakes of Slender Bodies," AIAA Journal, Vol 2, No. 2, February 1964.
19. Wilson, L. N.: Body Shape Effects on Axisymmetric Wakes, GM Defense Research Lab., TR64-02K, October 1964.
20. Proudian, A.; Feldman, S.; and Vas, I.: "A New Model for Mixing and Fluctuations in a Turbulent Wake," AIAA Journal, Vol 3, No. 4, p 602, April 1965.
21. Lees, L.; and Hromas, L.: "Turbulent Diffusion in the Wake of a Blunt-Nosed Body at Hypersonic Speeds," IAS Journal, p 976, August 1962.
22. Lykoudis, P.: The Growth of the Hypersonic Turbulent Wake Behind Blunt and Slender Bodies, RAND Corporation, RM-3270-PR, January 1963.
23. Slattery, R. E.; and Clay, W. G.: The Turbulent Wake of Hypersonic Bodies. ARS 2673-62, November 1962.
24. Lees, L.; and Reeves, B. L.: "Theory of Laminar Near Wake of Blunt Bodies in Hypersonic Flow," AIAA Journal, Vol 3, No. 11, November 1965.
25. Heinrich, H. G.; and Rust, L. W.: A Second Order Solution for the Velocity Distribution in a Turbulent Wake. FDL-TDR-64-156, April 1965.
26. Goulard, R.: A Preliminary Description of Re-Entry Wakes. Bendix Prob. Div., Res. Note 2, January 1960.

27. Zeiberg, S.; and Bleich, G.: A Finite-Difference Method Solution of the Laminar Hypersonic, Non-Equilibrium Wake. General Applied Science Laboratory (GASL), Technical Report No. 338, February 1963.
28. Ting, L.; and Libby, P.: Fluid Mechanics of Axisymmetric Wakes Behind Bodies in Hypersonic Flow. GASL, TR-145A, June 1960.
29. Kubota, T.; and Reeves, B. L.: "A Family of Similar Solutions for Axisymmetric Incompressible Wakes," AIAA Journal, Vol 2, No. 8, August 1964.
30. Steiger, M.; and Bloom, M.: "Three-Dimensional Effects in Viscous Wakes," IAS Journal, 62-102, June 1962.
31. Steiger, M.; and Bloom, M.: Velocities in Two-Dimensional Asymmetric Wakes, AFOSR1085, Brooklyn Polytech, July 1961.
32. Korkan, K. D.: An Integral Solution to the Two-Dimensional, High-Speed Wake, OSU Research Foundation, 1573-6, August 1964.
33. Nerem, R. M.: Supersonic Wake Phenomena with Application to Ballute-Type Decelerators. GER-11820, Goodyear Aerospace Corporation, November 1964.
34. Nerem, R. M.: An Approximate Method for Including the Effect of the Inviscid Wake on the Pressure Distribution on a Ballute-Type Decelerator, GER-11824, Goodyear Aerospace Corporation, November 1964.
35. Amsden, A. A.; and Harlow, F. H.: "Numerical Calculation of Supersonic Wake Flow," AIAA Journal, Vol 3, No. 11, November 1965.
36. McShera, J. T.: Wind Tunnel Pressure Measurements in the Wake of a Cone-Cylinder Model at Mach Numbers of 2.30 and 4.65, NASA TN D-2928, August 1965.
37. Todisco, A.; and Pallone, A. J.: "Near Wake Field Measurements," AIAA Journal, Vol 3, No. 11, November 1965.
38. McCarthy, J. F.; and Kubota, T.: "A Study of Wakes Behind a Circular Cylinder at  $M = 5.7$ ," AIAA Journal, Vol 2, No. 4, April 1964.
39. Charczenko, N.: Aerodynamic Characteristics Towed Spheres, Conical Rings and Cones Used as Decelerators at Mach Numbers from 1.57 to 4.65, NASA TN D-1789, April 1963.
40. Charczenko, N.; and McShera, J. T.: Aerodynamic Characteristics of Towed Cones Used as Decelerators at Mach Numbers from 1.57 to 4.65, NASA TN D-994, December 1961.

41. McShera, J. T.; and Keyes, W. J.: Wind Tunnel Investigation of a Balloon as a Towed Decelerator at Mach Numbers from 1.47 to 2.50, NASA TN D-919, June 1961.
42. McShera, J. T.: Aerodynamic Drag and Stability Characteristics of Towed Inflatable Decelerators at Supersonic Speeds, NASA TN D-1601, March 1963.
43. Bell, D. R.: Pressure Measurements on the Rigid Model of a Balloon Decelerator in the Wake of a Simulated Missile Payload at Mach Numbers 1.5 to 6.0, Arnold Engineering Development Center, AEDC-TDR-64-65, April 1964.
44. Heinrich, H. G.; and Hess, R. S.: Drag Characteristics of Several Two Body Systems at Transonic and Supersonic Speeds, RTD-TDR-63-4226, December 1964.
45. Heinrich, H. G.; Hess, R. S.; and Stumbris, G.: Drag Characteristics of Plates, Cones and Spheres in the Wake of a Cylindrical Body at Transonic Speeds, Research Technology Division, USAF, RTD-TDR-63-4023, January 1965.
46. Heinrich, H. G.; and Hess, R. S.: Drag Characteristics of Plates, Cones, Spheres, and Hemispheres in the Wake of a Forebody at Transonic and Supersonic Speeds, RTD-TDR-63-4242, December 1964.
47. Heinrich, H. G.; and Eckstrom, D. J.: Velocity Distribution in the Wake of Bodies of Revolution Based on Drag Coefficient, Aeronautical Systems Division, USAF, ASD-TDR-62-1103, December 1963.
48. Nebiker, F. R.; Jaremenko, I. M.; et al.: Aerodynamic Deployable Decelerator Performance Evaluation Program, Air Force Flight Dynamics Laboratory, AFFDL-TR-65-27, August 1965.
49. Sims, L. W.: The Effects of Design Parameters and Local Flow Fields on the Performance of Hyperflo Supersonic Parachutes and High Dynamic Pressure Parachute Concepts, AFFDL-TR-65-150, Vol I, September 1965.
50. Campbell, J. F.: Flow Field Survey and Decelerator Drag Characteristics in a Wake of 1/12 Scale Model of the X-15 Airplane at  $M = 2.30$  and 4.65, NASA TND, 1965.
51. Lin, C. C.: On the Stability of the Laminar Mixing Region Between Two Parallel Streams in a Gas, NACA-MIT, IN2887, January 1953.
52. Chapman, D. R.; Keuhn, D. M.; and Larson, H. K.: Investigation of Separated Flows in Supersonic and Subsonic Streams with Emphasis on the Effect of Transition, NACA Report 1356, 1958.

53. Perkins, T. M.; and Brice, T. R.: Static Stability Characteristics of the ALARR Booster and the Effect of the Payload Wake on a Full-Scale Ballute at Supersonic Speeds, AEDC-TR-66-36, February 1966.
54. Lykoudis, P. S.: A Review of Hypersonic Wake Studies, The Rand Corporation, RM-4493 ARPA, May 1965.
55. Levensteins, Z. J.; and Krumins, M. V.: Experimental Study of Aerodynamic Characteristics of Hypersonic Wakes, AIAA, 66-53, January 1966.
56. Kayser, L. D.: Pressure Distribution, Heat Transfer, and Drag Tests on the Goodyear Ballute at Mach 10, AEDC-TDR-62-39.
57. Uselton, J. C.; and Hahn, J. S.: Drag Characteristics of Three Ballute Decelerators in the Wake of the ALLAR Payload at Mach Numbers 2 to 4, AEDC-TR-65-218, October 1965.
58. Lowry, J. F.: Aerodynamic Characteristics of Various Types of Full Scale Parachutes at Mach Numbers 1.8 to 3, AEDC-TDR-64-120.
59. Reichenau, D. E. A.: Aerodynamic Performance of Various Hyperflo and Hemisflo Parachutes at Mach Numbers from 1.8 to 3, AEDC-TR-65-57, March 1965.